RESEARCH PAPER

DESIGN, SYNTHESIS AND IN SILICO ANALYSIS OF NOVEL SUBSTITUTED THIAZOLE DERIVATIVES FOR POTENTIAL INHIBITOR OF DIHYDROFOLATE REDUCTASE (DHFR)

Jayshree S. Kokat[1*], Sanjay B. Bhawar[2]
[1]Department of pharmaceutical chemistry, Research scholar Bhagwant University, Ajmer
[2]Professor, Pravara Rural College of Pharmacy, Loni, Maharashtra, India

Corresponding Author
Jayshree Sudhakar Kokat
Department of Pharmaceutical Chemistry
Affiliation: Research scholar Bhagwant university, Ajmer
Email Id: jayshreekokat4@gmail.com
Mo No.: 8308210177

Abstract
Objectives: Resistance in *Staphylococcus aureus* has eroded the value of antifolate antibacterials, creating a need for chemically distinct inhibitors of the same target. Twenty-five substituted thiazoles, varied independently at the thiazole C-2 position and anilide ring, were designed, synthesised and profiled against bacterial dihydrofolate reductase (DHFR).
Methods: TB1–TB25 were prepared by Hantzsch cyclisation of 4-(2-bromoacetyl)benzoic acid with twenty-five carbothioamides, then acid chloride activation and coupling with substituted anilines. Structures were confirmed by FT-IR, ^{1}H NMR, ^{13}C NMR and ESI-MS. ForceADME and Geintox-II predicted drug-likeness, pharmacokinetics and toxicity; docking against S. aureus DHFR (PDB ID: 2 W9H) used GeinDock Suite v2.5.8.0 with trimethoprim as reference.
Results: Nine top ranked derivatives were isolated from 72 to 80% yields (molecular weight ranging from 378.43 to 495.55 g/mol; LogP values ranging from 0.02 to 3.31); all compounds possessed one Lipinski violation and complete Veber compliance. Twenty four exhibited high absorption potential and twenty compounds fell within GHS classification level 4 and demonstrated lack of carcinogenicity, mutagenicity, cytotoxicity and immunotoxicity. Docking results indicated these twenty five molecules bound below trimethoprim at −6.730 kcal mol−1 and ranged from −8.215 to −9.715 kcal mol−1. Through cascade filtering based upon binding affinity, absorption profiles, toxicity levels and structural alerts, nine lead candidates emerged including TB10 at −9.672 kcal mol−1, TB22 at −9.586 kcal mol−1, TB4 at −9.433 kcal mol−1 and TB24 at −9.377 kcal mol−1. TB10 interacted through hydrogen bonding interactions involving residues THR46, THR121, GLN95 and ARG57 located along the hydrophobic channel of LEU20, LEU28, VAL31, ILE50, LEU54 and PHE92.
Conclusion: TB10, TB22, TB4 and TB24 exhibit highest predicted affinity towards Dihydrofolate Reductase (DHFR) while also displaying acceptable oral drug like qualities and low toxicological profile. These compounds occupy the folic cavity without engaging with residue Asp27 utilized by dipyrimidine analogues and therefore warrant further scale up for in vitro antibacterial and enzymatic inhibition studies.
Keywords: Thiazole; Benzanilide; Dihydrofolate reductase; Antibacterial; Molecular docking; In silico ADME
How to cite this article: Kokat JS, Bhawar SB. Design, synthesis and in silico analysis of novel substituted thiazole derivatives for potential inhibitor of dihydrofolate reductase (DHFR). Int J Drug Deliv Technol. 2026;16(75s): 278-302. DOI: 10.25258/ijddt.16.75s.33

Introduction

Bacterial infections which are no longer responsive to initial therapy constitute a defining clinical challenge for the present decade [1, 2]. Amongst these infections, Methicillin resistant Staphylococcus aureus (MRSA) in particular has acquired resistance determinant at such a rapid rate that introduction of novel antibiotic chemotypes has failed to keep pace [3]. Lineages resistant to methicillin and also exhibiting multiple drug resistances are currently endemic both within hospitals and communities. Consequences attributable to this problem extend beyond failures of treatment; admission periods lengthen and resort to agents with low therapeutic indices often ensues; additionally there is a heavy financial burden borne disproportionately by those healthcare systems which cannot afford to bear this burden [4, 5]. Resistance does not result from singular lesions but rather through concerted action including mutations at sites of target specificity, enzymatic inactivation

and upregulation of efflux coupled with tolerance due to biofilm formation [6, 7]. Incremental modifications to scaffolds thus yield diminishing benefits until eventually they are rendered ineffective. Therefore reliance upon genuinely new chemical entities targeting well defined essential bacterial targets continues to represent the most reliable way to extricate oneself from current impasses [8, 9].

Dihydrofolate reductase occupies a unique place amongst such targets; the enzyme catalyzes reduction of dihydrofolate into tetrahydrofolate via a step dependent on NADPH which serves as sole source of reduced folate cofactors for bacteria and production of these products is essential for synthesis of thymidylate, purines and methionine [10, 11]. Hence inhibition directly prevents DNA replication rather than merely slowing growth; however selective differentiation between bacterial and human enzymes has already proven successful clinically using dapsone derivatives [12, 13]. This prior success presents present difficulties because selection of resistance substitutions significantly diminishes potency of trimethoprim against recent isolates of Staphylococcus species. Consequently inhibitors which fill cavity differently through distinct signatures of hydrogen bonding and hydrophobic interactions prove of great interest since they are less likely to recognize substitutions selected under pressure exerted by dapsone derivatives [14, 15].

Starting from 1,3 thiadiazole rings is appropriate for such an undertaking; the nitrogen atom within the ring serves as competent acceptor of hydrogen bonds; sulfur atoms contribute to the surface with charge polarization which further complements hydrophobic sites on proteins and overall aromatic systems participate readily in π stacking interactions and π alkyl contacts [16, 17]. Metabolically stable and synthetically facile these rings have been widely used in pharmaceuticals targeting diverse indications including antibacterials, antifungals and anticancer drugs [18, 19]. Through coupling of thiophene moiety at carbon number four to benzoic acid followed by attachment of another aromatic ring via nitrogen of the amide linkage resulting architecture exhibits geometry that closely matches elongated channels of bacterial dihydrofolate reductase [20, 21]. Carbonyl group and NH groups serve together as donors and acceptors located centrally along the axis whereas terminal substituent positions separately and thus can be varied independently.

This motivation stems from prior studies in this scaffold wherein the 2 carbon position has been consistently fixed at methyl and variation occurs exclusively upon anilide ring [22, 23]. This limitation restricted accessibility of chemical space and neglected exploration along the C2 vector [24, 25]. Here a different approach introduces substituents at the 2 carbon position directly from components of the Hantzsch condensation thereby making these positions independent vectors of diversity traversing saturated heterocycles, strained small rings, fluorine substituents, sulfoxides, sulfonamides and basic amines. Twenty five compounds have been designed based upon this rationale synthesized characterized spectroscopically and evaluated computationally for drug likeness pharmacokinetics behavior predicted toxicity and binding affinities toward S aureus DHFR [26, 27]. It aims also to identify suitable candidate compounds for further laboratory experimentation and to define those combination of substitutions at 2 carbon and aniline which result in productive interactions within folic acid binding cavities.

Materials and Methods

Materials

Acetylbenzene-1-carboxylic acid of analytical standard (molecular weight 243.06 g/mol) was acquired from Sciquaint Chemicals based at Pune, India. Twenty five carbothioamide compounds substituting at the thiazole C2 site (of analytical standard, purity exceeding 98%) and twenty five corresponding anilines coupling partners (of analytical standard, purity exceeding 98%) were sourced from Research Lab Fine Chemicals Industries based at Pune, India. Sodium bicarbonate of analytical grade (purity greater than 99%), thionyl chloride of analytical grade (purity greater than 99%) and triethylamine of analytical grade (purity greater than 99%) were purchased from Neeta Chemicals also located at Pune India. Solvents such as dimethyl formamide free from water content (greater than 99.8% purity), dry toluene of HPLC grade and dichloromethane of HPLC grade together with ethanol of analytical purity (higher than 99.9%) which served as reaction media were obtained from Sciquaint Innovations OPC Pvt. Ltd. also situated at Pune India. KBr spectroscopically pure (purity higher than 99%) was obtained from Sciquaint Chemicals also at Pune India for making pellets for FT IR spectroscopy; CD Cl3 of NMR grade containing more than 99.8% by atom and DMSO d six of NMR grade having more than 99.9% by atom were also received from Sciquaint Chemicals also based in Pune India. Other chemicals and reagents utilized in the present study were of analytical standards and employed without additional purification except where otherwise stated.

Methods

Drug-Likeness and In-Silico ADME Prediction

Designed derivatives TB1 through TB25 were evaluated for drug likeness and pharmacokinetic behavior via the online computational platform ForceADME developed by Geinforce Technology Pvt. Ltd., located at Pune, India. Submission of two dimensional SMILES strings for each compound resulted in return of Lipinski Rule of Five descriptors including molecular weight, LogP value, number of hydrogen bond donors and hydrogen bond acceptors alongside Veber descriptors such as number of rotatable bonds and topological polar surface area. Profiles related to gastrointestinal absorption, penetration across blood brain barrier, substrates of P glycoproteins, inhibition profiles for cytochromes P450 (CYP 1 A2, CYP 2C19, CYP 2C9, CYP 2D6 and CYP 3 A4), skin permeability coefficient (log Kp) and an abbreviated measure of bioavailability were computed simultaneously. Retrieval also included compliance against Ghose, Egan and Muegge filters, quantitation of drug likeness scores, PAINS alerts and synthetic accessibilities. Reference standard treatment was maintained consistent with that applied to trimethoprim.

Toxicity Prediction

Silico toxicity assessments for all designed compounds were conducted using Geintox II, a web server for toxicological prediction that has been developed by Geinforce Technology Pvt. Ltd. located in Pune, India. SMILES representation of each compound was submitted to the tool which then predicted acute oral toxicity via median lethal dose (LD 50, mg/kg) along with corresponding Globally Harmonized System (GHS) classification and specific endpoints including hepatotoxicity, carcinogenesis, mutagenicity, cytotoxicity, clinical toxicity, immunotoxicity, nephrotoxicity, cardiovascular toxicity, neurological toxicity, respiratory toxicity, sensitization of skin, developmental toxicity, endocrine disruption, phospholipidosis and ecotoxicity as well as penetration through blood brain barrier [28, 29]. For each endpoint, results were reported as either positive or negative calls together with probability scores and ratings of reliability based on validated alerts derived from literature.

Ligand Preparation

Structures of all twenty five designed compounds TB1 through TB25 together with that of reference compound trimethoprim have been drawn using ChemDraw Professional software (Perkin Elmer Inc., United States). Prior to exporting, each structure has been checked for appropriate valences, orders of bonding and stereochemistry. Structures have then been saved in MOLEL format. Files in MOL format have subsequently been imported into GeM Dock Suite version 2.5.8.0. Hydrogens have been added at physiologically relevant pH 7.4 and each structure minimized by means of MMFF94 force field to reduce strain related to bond length, angle torsion and lack of contact. Partial atomic charges were also assigned and rigid bonds retained; resulting minimization conformations were then exported to PDBQT format thereby producing a set of twenty six ligands which are now prepared.

Selection of Target Receptor

Crystal structures of Staphylococcus aureus dihydrofolate reductase (DHFR; PDB ID: 2 W9H) were chosen as receptors for subsequent docking studies. DHFR catalyzes reduction of dihydrofolate to tetrahydrofolate utilizing NADPH thereby being essential for folate metabolism and synthesis of reduced cofactors necessary for biosynthesis of thymidylic acid, purines and methionine which arrest replication of DNA; inhibition of such enzyme constitutes an established antibacterial strategy. Structure captured from crystallization using 2 W9H contains wild type enzyme along with complexes of NADPH and a co crystallized dipyrimidinediamine inhibitor whereby cavities related to binding of folates, residues including acidic residue Asp27, hydroxylation networks involving Thr46, Ser49 and Thr121 and shelves contributed by Leu5, Val6, Ala7, Ile14, Leu20, Leu28, Val31, Phe92 and Phe98 are characterized experimentally. Docking employed scaffolds bearing thiazoles due to geometrical complementarity of these molecules to elongated channels of folates and distinct addressing of adjacent hydrophobic sites and solvent exposed regions through respective terminal substituent groups.

Protein Preparation

Three dimensional crystal structures of S. aureus DHFR have been retrieved from RCSB Protein Data Bank via its URL https://www.rcsb.org/. Retrieval is reported here as having been conducted by means of PDB format download. Following retrieval, processing took place utilizing Geindock Suite version 2.5.8.0. Chain A alone has been retained; removal also included all crystallization water molecules along with heteroatoms such as co crystallized inhibitors. Polar hydrogen atoms have subsequently been added based on standard protonation states at pH 7.4 and partial charges according to Gasteiger and Kollman have been assigned [30, 31]. Side chains located within cavity boundaries that border active site have been designated as flexible and the resulting receptor has been prepared into paired rigid and flexible PDBQT file formats for docking calculations. Furthermore, after processing further inspection of

the processed structure has taken place through BIOVIA Discovery Studio Visualizer version 4.5.

Molecular Docking

All twenty-five derivatives and trimethoprim underwent molecular docking using GeinDock Suite version 2.5.8.0 via the AutoDock Vina engine version 1.2.7 and through usage of Vina scoring functions. Prepared receptor and ligand PDBQT files were uploaded into the application interface and the search space was delineated based upon crystallographic covalent inhibitors coordinates with a pad of 12.0 Å; resulting in a central grid point located at x = 8.960 Å, y = -5.920 Å, and z = 16.430 Å with dimensions of 20.00 × 21.80 × 21.80 Å (volume 9504.80 Å³) and a spacing of 0.375 Å. Docking was executed at exhaustiveness level of 16 and generation of up to fifteen distinct binding modes for each ligand and distribution among 28 CPU cores. Prior to performing tests on chemical probes docking procedure was validated by redocking of the crystallized inhibitor onto the same grid under five different independent configurations [32, 33]. Grid acceptance criteria involved correction of symmetry followed by root mean square deviation less than 2.0 Å between redocked and experimental poses. Ranking of binding modes proceeded according to scores obtained in units of kcal/mol and retention of highest ranking conformations served for further analyses of intermolecular interactions [34, 35]. Using interaction module of GeinDock Suite both hydrogen bonds and weak C—H···O hydrogen bonds along with hydrophobic and alkyl contact relationships, π stacking and threading interactions, π cation and π anion contacts, salt bridges and halogen bonding interactions were identified. Two dimensional interaction diagrams and three dimensional pose figures produced herein reproduce these results.

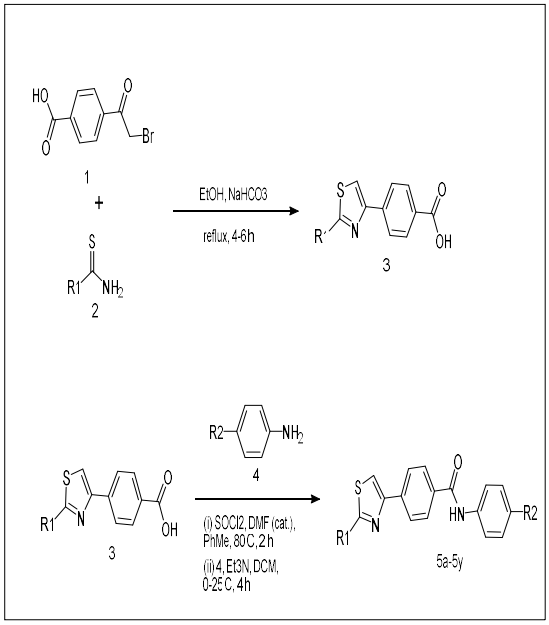

Figure 1: Proposed scheme II for synthesis of substituted thiazole derivatives

Table 1: Designed novel substituted thiazole derivatives (TB1–TB25) with the corresponding carbothioamide component defining the thiazole C-2 substituent, the aniline R-substitution and the IUPAC names of the final products synthesized via Scheme II.

Label	Carbothioamide (sets C-2)	Aniline R-substitution	IUPAC name of final product
TB1	Cyclopropanecarbothioamide	4-(morpholin-4-yl)	4-(2-cyclopropyl-1,3-thiazol-4-yl)-N-[4-(morpholin-4-yl)phenyl]benzamide
TB2	Oxane-4-carbothioamide	3-(dimethylphosphoryl)	N-[3-(dimethylphosphoryl)phenyl]-4-[2-(oxan-4-yl)-1,3-thiazol-4-yl]benzamide
TB3	Morpholine-4-carbothioamide	4-(methanesulfonyl)	N-[4-(methanesulfonyl)phenyl]-4-[2-(morpholin-4-yl)-1,3-thiazol-4-yl]benzamide
T	Oxetane-3-	3-fluoro-	N-[3-fluoro-4-

B 4	carbothioamide	4-(4-methylpiperazin-1-yl)	(4-methylpiperazin-1-yl)phenyl]-4-[2-(oxetan-3-yl)-1,3-thiazol-4-yl]benzamide
TB 5	Bicyclo[1.1.1]pentane-1-carbothioamide	4-(oxetan-3-yloxy)	4-[2-(bicyclo[1.1.1]pentan-1-yl)-1,3-thiazol-4-yl]-N-[4-(oxetan-3-yloxy)phenyl]benzamide
TB 6	3,3,3-Trifluoropropanethioamide	3-(difluoromethoxy)	N-[3-(difluoromethoxy)phenyl]-4-[2-(2,2,2-trifluoroethyl)-1,3-thiazol-4-yl]benzamide
TB 7	2,2-Difluoroethanethioamide	4-(1-methyl-1H-pyrazol-4-yl)	4-[2-(difluoromethyl)-1,3-thiazol-4-yl]-N-[4-(1-methyl-1H-pyrazol-4-yl)phenyl]benzamide
TB 8	2-Methoxyethanethioamide	4-(2-hydroxypropan-2-yl)	N-[4-(2-hydroxypropan-2-yl)phenyl]-4-[2-(methoxymethyl)-1,3-thiazol-4-yl]benzamide
TB 9	1-Methyl-1H-pyrazole-4-carbothioamide	3-(methanesulfonamido)	N-[3-(methanesulfonamido)phenyl]-4-[2-(1-methyl-1H-pyrazol-4-yl)-1,3-thiazol-4-yl]benzamide
TB 10	Pyrimidine-5-carbothioamide	4-(azetidine-1-carbonyl)	N-[4-(azetidine-1-carbonyl)phenyl]-4-[2-(pyrimidin-5-yl)-1,3-thiazol-4-yl]benzamide
TB 11	Azetidine-1-carbothioamide	3-cyano-4-fluoro	4-[2-(azetidin-1-yl)-1,3-thiazol-4-yl]-N-(3-cyano-4-fluorophenyl)benzamide
TB 12	4-Methylpiperazine-1-carbothioamide	4-(cyclopropanesulfonyl)	N-[4-(cyclopropanesulfonyl)phenyl]-4-[2-(4-methylpiperazin-1-yl)-1,3-thiazol-4-yl]benzamide
TB 13	Oxolane-3-carbothioamide	4-(oxan-4-yloxy)	N-[4-(oxan-4-yloxy)phenyl]-4-[2-(oxolan-3-yl)-1,3-thiazol-4-yl]benzamide
TB 14	1-Methylpiperidine-4-carbothioamide	3-methoxy-4-(morpholin-4-yl)	N-[3-methoxy-4-(morpholin-4-yl)phenyl]-4-[2-(1-methylpiperidin-4-yl)-1,3-thiazol-4-yl]benzamide
TB 15	Cyclobutanecarbothioamide	4-(3-hydroxyazetidin-1-yl)	4-(2-cyclobutyl-1,3-thiazol-4-yl)-N-[4-(3-hydroxyazetidin-1-yl)phenyl]benzamide
TB 16	1-(Trifluoromethyl)cyclopropane-1-carbothioamide	4-(N,N-dimethylsulfamoyl)	N-[4-(dimethylsulfamoyl)phenyl]-4-{2-[1-(trifluoromethyl)cyclopropyl]-1,3-thiazol-4-yl}benzamide
TB 17	2-Cyanoethanethioamide	4-(1,1-dioxo-1λ⁶-thiomorpholin-4-yl)	4-[2-(cyanomethyl)-1,3-thiazol-4-yl]-N-[4-(1,1-dioxo-1λ⁶-thiomorpholin-4-yl)phenyl]benzamide
TB 18	1-Methylazetidine-3-carbothioamide	4-(4-hydroxypiperidin-1-yl)	N-[4-(4-hydroxypiperidin-1-yl)phenyl]-4-[2-(1-methylazetidin

			-3-yl)-1,3-thiazol-4-yl]benzamide
TB19	2-Hydroxy-2-methylpropanethioamide	3-fluoro-4-(methanesulfonyl)	N-[3-fluoro-4-(methanesulfonyl)phenyl]-4-[2-(2-hydroxypropan-2-yl)-1,3-thiazol-4-yl]benzamide
TB20	Piperidine-1-carbothioamide	4-(2-methoxyethoxy)	N-[4-(2-methoxyethoxy)phenyl]-4-[2-(piperidin-1-yl)-1,3-thiazol-4-yl]benzamide
TB21	Pyrrolidine-1-carbothioamide	4-carbamoyl	N-(4-carbamoylphenyl)-4-[2-(pyrrolidin-1-yl)-1,3-thiazol-4-yl]benzamide
TB22	1-Methyl-1H-imidazole-4-carbothioamide	4-(pyrrolidine-1-sulfonyl)	4-[2-(1-methyl-1H-imidazol-4-yl)-1,3-thiazol-4-yl]-N-[4-(pyrrolidine-1-sulfonyl)phenyl]benzamide
TB23	Spiro[3.3]heptane-2-carbothioamide	4-(difluoromethyl)	N-[4-(difluoromethyl)phenyl]-4-[2-(spiro[3.3]heptan-2-yl)-1,3-thiazol-4-yl]benzamide
TB24	2-(Oxan-4-yl)ethanethioamide	3-(2-oxopyrrolidin-1-yl)	4-{2-[(oxan-4-yl)methyl]-1,3-thiazol-4-yl}-N-[3-(2-oxopyrrolidin-1-yl)phenyl]benzamide
TB25	3,3-Difluorocyclobutane-1-carbothioamide	4-(1H-pyrazol-1-yl)	4-[2-(3,3-difluorocyclobutyl)-1,3-thiazol-4-yl]-N-[4-(1H-pyrazol-1-yl)phenyl]benzamide

Synthesis and Characterization of Substituted Thiazole Derivatives

Nine derivatives which were prioritized through combined evaluation of absorption distribution metabolism and toxicity along with docking studies described subsequently have been advanced for further synthesis and spectroscopic characterization. Synthesis of each compound proceeded via two sequential steps: first, formation of thiazole ring together with its substituent at position 2 through cyclization using 4-(2 bromo acetyl) benzoic acid and appropriate carbathio amide; secondly activation of resulting benzoic acid into its acid chlorides and subsequent coupling with corresponding anilines.

Synthesis of N-[3-fluoro-4-(4-methylpiperazin-1-yl)phenyl]-4-[2-(oxetan-3-yl)-1,3-thiazol-4-yl]benzamide (TB4)

In a 100 mL round bottom flask, 4-(2-bromoisobutyrate) benzoic acid (0.243 g, 1.0 mmol) and oxetane 3 carbothioamide (0.117 g, 1.0 mmol) were dissolved in pure ethanol (15 mL) and sodium bicarbonate (0.084 g, 1.0 mmol) was added in one portion. The resulting mixture was refluxed under heat treatment for 5 h; then cooling to ambient temperature followed by pouring into crushed ice. Precipitate formed which was isolated by filtration, washed with cold water and air dried to afford 4 [2 (oxetanyl) -1, 3 thiadiazolyl] benzoic acid (0.209 g, 80% yield). An intermediate (0.261 g, 1.0 mmol) was dispersed in dry toluene (15 mL) along with a catalytic amount of dimethylformamide (2 drops) and sulfuric anhydride (0.145 mL, 2.0 mmol) was added dropwise and refluxing at 80 °C continued under nitrogen atmosphere for 2 h. Solvent together with superfluous sulfuric anhydride was removed via vacuum reduction and residual acid chlorides were dissolved in dry dichloromethane (10 mL). Separately, 3 fluorinated 4 (4 methyl piperazine) aniline (0.209 g, 1.0 mmol) was dissolved in dichloromethane (10 mL) that contained triethyl amine (0.28 mL, 2.0 mmol) and cooled to 0 °C. Solution of acid chlorides was subsequently added dropwise and stirring occurred at room temperature for 4 h. Successive washing with aqueous sodium carbonate solution, dilute hydrochloric acid and salt solution followed by drying over anhydrous sodium sulfate and concentration under reduced pressure resulted in crystallisation using ethanol.

Off-white solid; Yield: 0.353 g (78%); m.p. 196–199 °C. FT-IR (KBr) (cm^{-1}): 3302.46 (N-H amide), 3068.24 (Ar-H), 2942.18 (C-H aliphatic), 2801.34 (N-CH_3), 1654.72 (C=O amide), 1602.38 (C=C aromatic), 1538.64 (C=N thiazole), 1322.47 (C-N), 1268.53 (C-F), 1146.28 (C-N piperazine), 978.36 (C-O-C oxetane), 832.14 (C-H out-of-plane). ^1H

NMR (500 MHz, $CDCl_3$) δ: 9.82 (s, 1H, NH), 8.06 (d, J = 8.5 Hz, 2H, Ar-H), 7.92 (d, J = 8.5 Hz, 2H, Ar-H), 7.58 (dd, J = 14.2, 2.4 Hz, 1H, Ar-H), 7.46 (s, 1H, thiazole-H), 7.16 (dd, J = 8.7, 2.4 Hz, 1H, Ar-H), 6.96 (t, J = 9.0 Hz, 1H, Ar-H), 5.04 (t, J = 6.8 Hz, 2H, oxetane-OCH_2), 4.88 (t, J = 6.4 Hz, 2H, oxetane-OCH_2), 4.34 (quint, J = 6.6 Hz, 1H, oxetane-CH), 3.06 (m, 4H, piperazine-H), 2.58 (m, 4H, piperazine-H), 2.35 (s, 3H, N-CH_3). ^{13}C NMR (125 MHz, $CDCl_3$) δ: 170.86,165.34,155.42 (d, J = 245.6 Hz, C-F), 154.18,138.62,136.47 (d, J = 9.2 Hz), 135.04,133.58 (d, J = 10.4 Hz), 128.06,126.52,119.38 (d, J = 4.2 Hz), 115.46,114.72,107.94 (d, J = 26.3 Hz), 74.62, 55.24, 50.68 (d, J = 3.0 Hz), 45.92, 35.41. ESI-MS (m/z): 453.57 $[M+H]^+$.

Synthesis of 4-[2-(difluoromethyl)-1,3-thiazol-4-yl]-N-[4-(1-methyl-1H-pyrazol-4-yl)phenyl]benzamide (TB7)

In a 100 mL round bottom flask, 4-(2-Bromocaprylic acid) benzoic acid (0.243 g; 1.0 mmol) and 2,2 difluorothioacetamide (0.111 g; 1.0 mmol) were dissolved in absolute ethanol (15 mL) and sodium bicarbonate (0.084 g; 1.0 mmol) was added in one portion. The resulting mixture was refluxed under heat for 4 h and then cooled to ambient temperature before being poured into crushed ice. Precipitated solids were isolated by filtration, washed with cold water and subsequently dried which afforded 4 [2-(difluoromethyl)thiazol-4-yl] benzoic acid (0.209 g; 82% yield). An intermediate prepared (0.255 g; 1.0 mmol) was suspended in dry toluene (15 mL) along with catalytic amount of dimethylformamide (2 drops) and sulfate monochloride was added dropwise and refluxed at 80 °C under nitrogen atmosphere for 2 h. Solvent together with excess sulfate monochloride was removed under reduced pressure and residual acid chlorides were dissolved in dry dichloromethane (10 mL). Separately, 4 methyl pyrazol-4-yl aniline (0.173 g; 1.0 mmol) was dissolved in dichloromethane (10 mL) that contained triethylamine (0.28 mL; 2.0 mmol) and cooled to 0 °C. Residual acid chloride solution was added dropwise and stirring continued at room temperature for 4 h. Successive washes with aqueous sodium carbonate solution, dilute hydrochloric acid and brine followed by drying over anhydrous sodium sulfate under reduced pressure and recrystallization performed using ethanol yielded final product.

Pale yellow solid; Yield: 0.312 g (76%); m.p. 212–215 °C. FT-IR (KBr) (cm^{-1}): 3308.72 (N-H amide), 3086.45 (Ar-H), 2934.28 (C-H aliphatic), 1659.34 (C=O amide), 1606.82 (C=C aromatic), 1548.16 (C=N thiazole), 1496.73 (C=N pyrazole), 1316.24 (C-N), 1204.58 (C-F), 1078.43 (C-F_2), 826.37 (C-H out-of-plane). ^1H NMR (500 MHz, $CDCl_3$) δ: 9.88 (s, 1H, NH), 8.12 (d, J = 8.5 Hz, 2H, Ar-H), 7.94 (d, J = 8.6 Hz, 2H, Ar-H), 7.82 (s, 1H, pyrazole-H), 7.68 (s, 1H, pyrazole-H), 7.64 (s, 1H, thiazole-H), 7.58 (d, J = 8.7 Hz, 2H, Ar-H), 7.46 (d, J = 8.7 Hz, 2H, Ar-H), 6.92 (t, J = 53.6 Hz, 1H, CHF_2), 3.94 (s, 3H, N-CH_3). ^{13}C NMR (125 MHz, $CDCl_3$) δ: 165.48,163.24 (t, J = 32.4 Hz, thiazole C-2), 153.36,138.42,136.18,134.86,132.47,131.24,128.14 ,127.62,126.38,122.46,120.62,119.84,118.42,110.24 (t, J = 232.6 Hz, CHF_2), 39.18. ESI-MS (m/z): 411.46 $[M+H]^+$.

Synthesis of N-[4-(azetidine-1-carbonyl)phenyl]-4-[2-(pyrimidin-5-yl)-1,3-thiazol-4-yl]benzamide (TB10)

Aqueous dissolution occurred in a 100 mL round bottom flask where 4-(2 Bromo Acetic Acid) Benzoic Acid (0.243 g; 1.0 mmol) and Pyrimidine 5 Carbothioamide (0.139 g; 1.0 mmol) had been dissolved using absolute ethanol (15 mL); subsequently Sodium Bicarbonate (0.084 g; 1.0 mmol) was added in a single portion. Heating under reflux proceeded for 6 h; cooling ensued followed by pouring into crushed ice. Precipitate formed which was isolated via filtration, washed with cold water and then dried to yield 4 [2 (Pyrimidine 5 Yl) Thiazole 4 Yl] Benzoic Acid (0.215 g; 76%) as an intermediate product. Suspension formation took place in dry Toluene (15 mL) along with addition of Sulfuryl Chloride (0.145 mL; 2.0 mmol) and Dimethylformamide (Dmf) in catalytic amount. Refluxing at 80 °C under Nitrogen atmosphere proceeded for 2 h. Subsequently removal of solvent under vacuum coupled with dissolving residue into Dry Dichloromethane (10 mL) also took place. Separately in another flask Aminophenyl Azetidinyl Methanone (0.176 g; 1.0 mmol) was dissolved into Dichloromethane (10 mL) containing Triethylamine (0.28 mL; 2.0 mmol) and cooling to 0 °C ensued prior to addition of the residue of acid chloride solution. Stirring at ambient temperature continued for 4 h. Sequential washing with Saturation Sodium Hydrogen Carbonate Solution, Dilute Hydrochloric Acid and Salt Water followed by drying over Anhydrous Sodium Sulfate and concentration under reduced pressure also took place. Recrystallization from Ethanol concluded the process.

Off-white solid; Yield: 0.327 g (74%); m.p. 238–241 °C. FT-IR (KBr) (cm^{-1}): 3294.68 (N-H amide), 3078.52 (Ar-H), 2948.36 (C-H aliphatic), 1662.47 (C=O amide), 1628.34 (C=O azetidinyl amide), 1598.72 (C=C aromatic), 1552.18 (C=N thiazole), 1508.46 (C=N pyrimidine), 1324.63 (C-N), 1246.82 (C-N azetidine), 842.36 (C-H out-of-plane). ^1H NMR (500 MHz, $CDCl_3$) δ: 9.94 (s, 1H, NH), 9.28 (s, 1H, pyrimidine-H), 9.22 (s, 2H, pyrimidine-H), 8.14 (d, J = 8.5 Hz, 2H, Ar-H), 7.98

(d, J = 8.6 Hz, 2H, Ar-H), 7.74 (d, J = 8.7 Hz, 2H, Ar-H), 7.68 (s, 1H, thiazole-H), 7.58 (d, J = 8.7 Hz, 2H, Ar-H), 4.28 (t, J = 7.7 Hz, 2H, azetidine-H), 4.10 (t, J = 7.7 Hz, 2H, azetidine-H), 2.32 (quint, J = 7.7 Hz, 2H, azetidine-H). ^{13}C NMR (125 MHz, $CDCl_3$) δ: 169.42,168.36,165.62,158.24,154.86,153.12,140.28 ,138.64,134.92,129.86,128.42,127.18,126.54,124.3 2,119.68,116.24, 53.84, 49.72, 16.08. ESI-MS (m/z): 442.53 $[M+H]^+$.

Synthesis of N-[4-(cyclopropanesulfonyl)phenyl]-4-[2-(4-methylpiperazin-1-yl)-1,3-thiazol-4-yl]benzamide (TB12)

In a 100 mL round-bottom flask, 4-(2-bromoisocyanato) benzoic acid (0.243 g; 1.0 mmol) and 4 methyl piperazine carbothioamide (0.159 g; 1.0 mmol) were dissolved in absolute ethanol (15 mL) and sodium bicarbonate (0.084 g; 1.0 mmol) was added in one portion. The resulting mixture was refluxed for 6 h and then cooled to room temperature whereupon precipitation of solid occurred which was isolated by filtration and washed with cold water before drying and afforded 4 [2 (4 methyl piperazino) - 1H thiolo cycle 4 yl] benzoic acid (0.237 g; 78%). An intermediate thus obtained (0.303 g; 1.0 mmol) was suspended in dry toluene (15 mL) and reacted with dropwise addition of sulfate monochloride (0.145 mL; 2.0 mmol) along with a catalytic amount of dimethyl formamide (2 drops) and refluxed at 80 °C under nitrogen atmosphere for 2 h. Removal of solvent under reduced pressure along with excess sulfate monochloride resulted in formation of an acid chloride residue which was subsequently dissolved into dry dichloromethane (10 mL). Simultaneously another flask contained 4 cyclo propyl sulfino aniline (0.197 g; 1.0 mmol) dissolved in dichloromethane (10 mL) containing triethyl amine (0.28 mL; 2.0 mmol) and cooling to 0 °C. Slow addition of the acid chloride solution followed by stirring at room temperature for 4 h yielded the reaction mixture. This mixture underwent successive washing with aqueous sodium bicarbonate solution, dilute hydrochloric acid and saltwater, drying with anhydrous sodium sulfate and concentration under reduced pressure followed by crystallization using ethanol.

White solid; Yield: 0.372 g (77%); m.p. 204–207 °C. FT-IR (KBr) (cm^{-1}): 3286.34 (N-H amide), 3072.18 (Ar-H), 2938.62 (C-H aliphatic), 2794.46 (N-CH_3), 1656.28 (C=O amide), 1594.73 (C=C aromatic), 1536.42 (C=N thiazole), 1312.86 (C-N), 1286.34 (S=O asymmetric), 1142.57 (S=O symmetric), 1064.28 (C-SO_2), 848.36 (C-H out-of-plane). ^{1}H NMR (500 MHz, $CDCl_3$) δ: 9.76 (s, 1H, NH), 8.02 (d, J = 8.5 Hz, 2H, Ar-H), 7.94 (d, J = 8.6 Hz, 2H, Ar-H), 7.88 (d, J = 8.7 Hz, 2H, Ar-H), 7.82 (d, J = 8.7 Hz, 2H, Ar-H), 7.02 (s, 1H, thiazole-H), 3.58 (m, 4H, piperazine-H), 2.52 (m, 4H, piperazine-H), 2.48 (m, 1H, cyclopropyl-CH), 2.34 (s, 3H, N-CH_3), 1.34 (m, 2H, cyclopropyl-CH_2), 1.06 (m, 2H, cyclopropyl-CH_2). ^{13}C NMR (125 MHz, $CDCl_3$) δ: 170.24,165.38,150.86,143.62,138.46,135.12,133.84 ,129.62,128.34,127.06,119.48,103.82, 54.68, 47.92, 46.14, 32.68, 5.42. ESI-MS (m/z): 483.64 $[M+H]^+$.

Synthesis of 4-[2-(cyanomethyl)-1,3-thiazol-4-yl]-N-[4-(1,1-dioxo-1λ⁶-thiomorpholin-4-yl)phenyl]benzamide (TB17)

In a 100 mL round bottom flask 4-(2-Bromocarbonyl) benzoic acid (0.243 g, 1.0 mmol) and 2 cyano ethanethiol amide (0.1 g, 1.0 mmol) were dissolved into absolute ethanol (15 mL) and sodium bicarbonate (0.084 g, 1.0 mmol) was added in one portion; the resulting mixture was refluxed for 5 h and then cooled to ambient temperature and poured onto crushed ice. Precipitate formed which was isolated via filtration washing with cold water and subsequently drying afforded 4 [2 (cyanomethyl) 1, 3 thiadiazol 4 yl] benzoic acid (0.193 g, 79% yield). Intermediate obtained (0.244 g, 1.0 mmol) was suspended in dry toluene (15 mL) along with addition of a catalytic amount of dimethylformamide (2 drops) and dropwise addition of sulfate monochloride; the resultant mixture was refluxed at 80 °C for 2 h under nitrogen atmosphere. Solvent together with excess sulfate monochloride was removed by means of vacuum distillation and residual acid chloride was dissolved in dry dichloromethane (10 mL); separately 4 (1, 1 dioxo 1 λ six thiomorpholine 4 yl) aniline (0.226 g, 1.0 mmol) was dissolved into dichloromethane (10 mL) containing triethylamine (0.28 mL, 2.0 mmol) and cooled to 0 °C. Acid chloride solution was then added dropwise and stirring continued at ambient temperature for 4 h. Reaction mixture underwent sequential washes with aqueous sodium bicarbonate solution followed by dilute hydrochloric acid and brine; reaction was dried over anhydrous sodium sulfate and solvent concentration carried out under reduced pressure and recrystallization performed using ethanol.

Pale yellow solid; Yield: 0.330 g (73%); m.p. 246–249 °C. FT-IR (KBr) (cm^{-1}): 3312.58 (N-H amide), 3082.36 (Ar-H), 2946.72 (C-H aliphatic), 2254.18 (C≡N nitrile), 1648.64 (C=O amide), 1596.28 (C=C aromatic), 1542.83 (C=N thiazole), 1308.46 (C-N), 1288.34 (S=O asymmetric), 1124.62 (S=O symmetric), 836.28 (C-H out-of-plane). ^{1}H NMR (500 MHz, DMSO-d_6) δ: 10.18 (s, 1H, NH), 8.14 (s, 1H, thiazole-H), 8.02 (d, J = 8.5 Hz, 2H, Ar-H), 7.96 (d, J = 8.6 Hz, 2H, Ar-H), 7.68 (d, J = 8.9 Hz, 2H, Ar-H), 7.02 (d, J = 8.9 Hz, 2H, Ar-H), 4.42 (s, 2H, CH_2CN), 3.82 (m, 4H, thiomorpholine-NCH_2), 3.16 (m, 4H, thiomorpholine-SO_2CH_2). ^{13}C NMR

(125 MHz, DMSO-d_6) δ: 165.24,162.86,153.42,146.28,138.34,134.62,131.18 ,128.06,127.42,122.34,118.86,116.42,115.28, 50.24, 45.86, 23.14. ESI-MS (m/z): 453.57 $[M+H]^+$.

Synthesis of N-[4-(4-hydroxypiperidin-1-yl)phenyl]-4-[2-(1-methylazetidin-3-yl)-1,3-thiazol-4-yl]benzamide (TB18)

In a 100 mL round bottom flask 4-(2-Bromocarbonyl) benzoic acid (0.243 g; 1.0 mmol) and 1 methyl azetidine-3 carboxy thiourea (0.130 g; 1.0 mmol) were dissolved in pure ethanol (15 mL); 0.084 g of sodium bicarbonate in one portion was then added. The resulting mixture was refluxed for 5 h and subsequently cooled to ambient temperature before being poured into crushed ice. Precipitated solid was isolated by filtration and washed with cold water and dried to yield 4 [2 (1 Methyl Azetidine-3 Yl) 1, 3 Thiolo Zol 4 Yl] Benzoic Acid (0.211 g; 77%) which served as an intermediate. Said intermediate (0.274 g; 1.0 mmol) was suspended in dry toluene (15 mL) and addition of drop wise of a catalytic amount of dimethyl formamide (2 drops) followed by gradual refluxing at 80 °C for 2 h under nitrogen atmosphere. Under reduced pressure removal of solvent along with excess thionyl chloride afforded an acid chloride residue which was dissolved in dry dichloromethane (10 mL). Separately in another flask 1 (4 Amino Phenyl) Piperidine 4 Ol (0.192 g; 1.0 mmol) was dissolved in dichloromethane (10 mL) that also contained triethyl amine (0.28 mL; 2.0 mmol) and cooling to 0 °C. Slow addition of said acid chloride solution proceeded followed by stirring at room temperature for 4 h. Successive washing of the resultant mixture with aqueous sodium bicarbonate solution, dilute hydrochloric acid and brine ensued. Drying over anhydrous sodium sulfate led to concentration under reduced pressure and subsequent crystallization from ethanol.

Off-white solid; Yield: 0.336 g (75%); m.p. 218–221 °C. FT-IR (KBr) (cm^{-1}): 3386.24 (O-H), 3296.48 (N-H amide), 3064.72 (Ar-H), 2936.18 (C-H aliphatic), 2788.36 (N-CH_3), 1646.82 (C=O amide), 1598.24 (C=C aromatic), 1534.68 (C=N thiazole), 1318.42 (C-N), 1068.36 (C-O alcohol), 824.58 (C-H out-of-plane). ^{1}H NMR (500 MHz, DMSO-d_6) δ: 10.02 (s, 1H, NH), 8.06 (s, 1H, thiazole-H), 7.98 (d, J = 8.5 Hz, 2H, Ar-H), 7.92 (d, J = 8.6 Hz, 2H, Ar-H), 7.56 (d, J = 8.9 Hz, 2H, Ar-H), 6.92 (d, J = 8.9 Hz, 2H, Ar-H), 4.68 (d, J = 4.2 Hz, 1H, OH), 4.02 (m, 1H, azetidine-CH), 3.72 (t, J = 7.6 Hz, 2H, azetidine-H), 3.58 (m, 1H, piperidine-CHOH), 3.52 (m, 2H, piperidine-H), 3.36 (t, J = 7.4 Hz, 2H, azetidine-H), 2.72 (m, 2H, piperidine-H), 2.30 (s, 3H, N-CH_3), 1.82 (m, 2H, piperidine-H), 1.46 (m, 2H, piperidine-H). ^{13}C NMR (125 MHz, DMSO-d_6) δ: 171.86,165.18,154.24,147.62,138.42,134.86,130.24 ,128.12,127.36,122.48,116.84,115.42, 66.34, 61.28, 48.72, 46.18, 34.86, 32.42. ESI-MS (m/z): 449.60 $[M+H]^+$.

Synthesis of 4-[2-(1-methyl-1H-imidazol-4-yl)-1,3-thiazol-4-yl]-N-[4-(pyrrolidine-1-sulfonyl)phenyl]benzamide (TB22)

In a 100 mL round bottom flask, 4-(2-Bromoisobutyryl) benzoic acid (0.243 g; 1.0 mmol) and 1-Methyl-1 H imidazole-4 carbothioamide (0.141 g; 1.0 mmol) were dissolved into absolute ethanol (15 mL) and sodium bicarbonate (0.084 g; 1.0 mmol) was added in one portion. The resulting mixture was refluxed for 6 h and then cooled to room temperature before being poured into crushed ice. Precipitate formed which was isolated via filtration, washed with cold water and dried to afford 4-[2-(1 Methyl Imidazo l-4 Yl) -1, 3 Thiazolo 4 Yl] Benzoic Acid (0.214 g; 75%). An intermediate thus obtained (0.285 g; 1.0 mmol) was suspended in dry toluene (15 mL); addition of sulfuric anhydride (0.145 mL; 2.0 mmol) and trace amount of dimethyl formamide occurred gradually followed by refluxing at 80 °C under nitrogen atmosphere for 2 h. Subsequently solvent along with excess sulfuric anhydride was removed under vacuum and residue consisting of acid chlorides was solubilized in dry dichloromethane (10 mL). Separately pyridinium piperidine sulfinate (0.226 g; 1.0 mmol) was dissolved in dry dichloromethane (10 mL) and cooling to 0 °C and subsequently solution of acid chlorides was slowly added and stirring continued at room temperature for 4 h. Successive washing with aqueous sodium bicarbonate solution, dilute hydrochloric acid and brine took place followed by drying using anhydrous sodium sulfate and concentration under reduced pressure. Recrystallization was performed with ethanol.

White solid; Yield: 0.355 g (72%); m.p. 252–255 °C. FT-IR (KBr) (cm^{-1}): 3304.62 (N-H amide), 3076.48 (Ar-H), 2942.36 (C-H aliphatic), 1652.28 (C=O amide), 1600.84 (C=C aromatic), 1546.32 (C=N thiazole), 1492.18 (C=N imidazole), 1326.74 (S=O asymmetric), 1310.42 (C-N), 1156.28 (S=O symmetric), 1092.36 (S-N sulfonamide), 830.62 (C-H out-of-plane). ^{1}H NMR (500 MHz, DMSO-d_6) δ: 10.52 (s, 1H, NH), 8.22 (s, 1H, thiazole-H), 8.06 (d, J = 8.5 Hz, 2H, Ar-H), 7.98 (d, J = 8.6 Hz, 2H, Ar-H), 7.86 (s, 1H, imidazole-H), 7.82 (d, J = 8.8 Hz, 2H, Ar-H), 7.76 (s, 1H, imidazole-H), 7.72 (d, J = 8.8 Hz, 2H, Ar-H), 3.74 (s, 3H, N-CH_3), 3.14 (m, 4H, pyrrolidine-NCH_2), 1.68 (m, 4H, pyrrolidine-CH_2). ^{13}C NMR (125 MHz, DMSO-d_6) δ: 165.46,163.28,154.12,143.86,138.62,136.24,134.48 ,132.16,129.84,128.36,127.42,122.68,119.24,116.8

2, 47.86, 34.28, 25.14. ESI-MS (m/z): 494.62 $[M+H]^+$.

Synthesis of 4-{2-[(oxan-4-yl)methyl]-1,3-thiazol-4-yl}-N-[3-(2-oxopyrrolidin-1-yl)phenyl]benzamide (TB24)

In a 100 mL round bottom flask 4-(2-Bromocaproic acid) benzoate (0.243 g; 1.0 mmol) and 2 oxazinan-4-yl ethanethiol amide (0.159 g; 1.0 mmol) were dissolved in absolute ethanol (15 mL) and sodium bicarbonate (0.084 g; 1.0 mmol) was added in a single portion. The resulting mixture was refluxed for 5 h and then cooled to ambient temperature whereupon precipitation of solid occurred which was isolated by filtration after washing with cold water and drying to yield 4 {2 [(oxazinan-4-yl] methylthio}-1, 3 thiadiazole benzoyl acid (0.246 g; 81%). An intermediate thus obtained (0.303 g; 1.0 mmol) was suspended in dry toluene (15 mL) and addition was made dropwise of sulfate monochloride (0.145 mL; 2.0 mmol) along with a catalytic amount of dimethyl formamide (2 drops). Under nitrogen atmosphere at refluxing temperature at 80 °C reaction proceeded for 2 h. Removal of residual solvent under vacuum afforded residue that was subsequently dissolved into dry dichloromethane (10 mL). Separately, 1 (3 amino phenyl) pyrrolidine-2 one (0.176 g; 1.0 mmol) was dissolved into dry dichloromethane (10 mL) containing triethylamine (0.28 mL; 2.0 mmol) and cooled to 0 °C. Slow addition of the acid chloride solution followed by stirring at room temperature for 4 h resulted in completion of reaction. Sequential washes with aqueous sodium bicarbonate solution, dilute hydrochloric acid and aqueous phase separation and drying over anhydrous sodium sulfate followed by concentration under reduced pressure and crystallisation using ethanol led to purification.

Off-white solid; Yield: 0.365 g (79%); m.p. 188–191 °C. FT-IR (KBr) (cm^{-1}): 3288.46 (N-H amide), 3066.28 (Ar-H), 2928.64 (C-H aliphatic), 2852.18 (C-H aliphatic), 1682.34 (C=O lactam), 1656.72 (C=O amide), 1596.48 (C=C aromatic), 1540.26 (C=N thiazole), 1320.84 (C-N), 1136.42 (C-O-C oxane), 1092.36 (C-O), 838.24 (C-H out-of-plane). ^{1}H NMR (500 MHz, $CDCl_3$) δ: 9.78 (s, 1H, NH), 8.08 (d, J = 8.5 Hz, 2H, Ar-H), 7.92 (d, J = 8.6 Hz, 2H, Ar-H), 7.86 (t, J = 2.0 Hz, 1H, Ar-H), 7.52 (dd, J = 8.1, 2.0 Hz, 1H, Ar-H), 7.44 (s, 1H, thiazole-H), 7.42 (dd, J = 8.1, 2.0 Hz, 1H, Ar-H), 7.36 (t, J = 8.1 Hz, 1H, Ar-H), 3.98 (dd, J = 11.4, 3.8 Hz, 2H, oxane-OCH_2), 3.86 (t, J = 7.1 Hz, 2H, pyrrolidinone-NCH_2), 3.38 (td, J = 11.6, 2.2 Hz, 2H, oxane-OCH_2), 2.98 (d, J = 7.0 Hz, 2H, thiazole-CH_2), 2.62 (t, J = 8.1 Hz, 2H, pyrrolidinone-CH_2), 2.18 (quint, J = 7.6 Hz, 2H, pyrrolidinone-CH_2), 2.02 (m, 1H, oxane-CH), 1.68 (m, 2H, oxane-CH_2), 1.42 (m, 2H, oxane-CH_2). ^{13}C NMR (125 MHz, $CDCl_3$) δ: 174.28,168.42,165.34,154.06,139.86,138.54,134.72,129.48,128.16,127.32,122.64,118.42,116.28,113.86, 67.84, 48.92, 41.24, 38.62, 34.18, 32.86, 18.06. ESI-MS (m/z): 462.60 $[M+H]^+$.

Synthesis of 4-[2-(3,3-difluorocyclobutyl)-1,3-thiazol-4-yl]-N-[4-(1H-pyrazol-1-yl)phenyl]benzamide (TB25)

In a 100 mL round bottom flask, 4-(2 bromo acetic acid) benzoic acid (0.243 g, 1.0 mmole) along with 3,3 disubstituted cyclobutane carbothioamide (0.151 g, 1.0 mmole) were dissolved in absolute ethanol (15 mL); subsequently sodium bicarbonate (0.084 g, 1.0 mmole) was added in one portion. The resulting mixture was refluxed for 4 h; cooling to room temperature followed by pouring into crushed ice produced solid precipitation which was isolated through filtration and purified by washing with cold water before drying to yield 4 [2 (3,3 disubstitution cyclobutyl) 1, 3 thiazol-4 yl] benzoic acid (0.245 g, 83% yield). Intermediate obtained (0.295 g, 1.0 mmole) was dispersed in dry toluene (15 mL) and addition of sulfate monochloride (0.145 mL, 2.0 mmole) along with catalytic amount of dimethyl formamide (2 drops) proceeded dropwise and resulted in refluxing at 80 °C under nitrogen atmosphere for 2 h. Subsequently removing residual solvent under vacuum and dissolving the resultant acid chlorides in dry dichloromethane (10 mL) further ensued. Separately 4 (1 H pyrazole 1 yl) aniline (0.159 g, 1.0 mmole) was dissolved in dry dichloromethane (10 mL) containing triethyl amine (0.28 mL, 2.0 mmole) and cooled to 0 °C. Acid chlorides solution was slowly added and stirring occurred at ambient temperature for 4 h. Resultant mixture underwent successive washing with aqueous sodium carbonate solutions, dilute hydrochloric acids and saltwater, drying using anhydrous sodium sulfate and concentration under reduced pressure followed by recrystallization using ethanol.

Pale yellow solid; Yield: 0.349 g (80%); m.p. 224–227 °C. FT-IR (KBr) (cm^{-1}): 3296.72 (N-H amide), 3082.46 (Ar-H), 2948.28 (C-H aliphatic), 1658.34 (C=O amide), 1604.62 (C=C aromatic), 1544.18 (C=N thiazole), 1512.36 (C=N pyrazole), 1318.24 (C-N), 1218.68 (C-F), 1084.42 (C-F_2), 844.36 (C-H out-of-plane). ^{1}H NMR (500 MHz, $CDCl_3$) δ: 9.86 (s, 1H, NH), 8.10 (d, J = 8.5 Hz, 2H, Ar-H), 7.94 (d, J = 8.6 Hz, 2H, Ar-H), 7.92 (d, J = 2.4 Hz, 1H, pyrazole-H), 7.76 (d, J = 8.8 Hz, 2H, Ar-H), 7.74 (d, J = 1.7 Hz, 1H, pyrazole-H), 7.68 (d, J = 8.8 Hz, 2H, Ar-H), 7.42 (s, 1H, thiazole-H), 6.48 (t, J = 2.1 Hz, 1H, pyrazole-H), 3.72 (m, 1H, cyclobutyl-CH), 3.02 (m, 2H, cyclobutyl-CH_2), 2.72 (m, 2H, cyclobutyl-CH_2). ^{13}C NMR (125 MHz, $CDCl_3$) δ: 171.62,165.28,154.34,141.86,138.42,136.24,134.68,128.24,127.46,126.82,121.34,120.48,119.62,116.2

8 (t, J = 274.2 Hz, CF_2), 108.24, 38.62 (t, J = 24.6 Hz), 29.84. ESI-MS (m/z): 437.50 $[M+H]^+$.

Results and Discussion

Results

Calculations of Lipinski's rule of Five and Druglikeness

Table 2 collects together Lipinski rules of 5 and Veber parameters computed for each of twenty five compounds designated TB1 through TB25 along with the reference standard trimethoprim. Molecular weight ranges from 378.43 g mol^{-1} (for TB11) to 495.55 g mol^{-1} (for TB16); thus these values fall consistently under the maximum limit of 500 g mol^{-1} across the series. Values for LogP range between 0.02 (compound TB9) and 3.31 (TB6). Moderation of lipophilicity which results from introduction of saturated heteroaryl groups and sulfonate substituents at position 2 and on the aniline ring has been successful as indicated by compliance within the upper limit of 5. Counts of hydrogen bond acceptors vary from three (TB23) to seven (TB3, TB9, TB12, TB17 and TB22) while those of donors are either one or 2 and hence fully compliant with acceptable limits. Variation in topological polar surface area spans from 41.99 $Å^2$ (TB23) to 105.98 $Å^2$ (TB9) whereas variation in number of rotatable bonds varies from four (TB11) to ten (TB8). Accordingly each compound meets the criterion of having fewer than ten rotatable bonds and polar surface area below 140 $Å^2$. One violation according to XLOGP3 WLOGP lipophilicity calculation occurs for each compound and also for trimethoprim; therefore the series remains equally compliant with respect to established rules.

Table 2: Lipinski's Rule of Five and Veber's Rule Parameters for All Compounds

Compound Name	M Log P	Mol. Wt. (g/mol)	HBA	HBD	Violations	Total Polar Surface Area ($Å^2$)	No. of Rotatable Bonds
TB1	2.05	405.52	5	1	1	54.46	5
TB2	2.32	440.5	5	1	1	68.29	7
TB3	1.97	443.55	7	1	1	88.6	6
TB4	2.05	452.55	6	1	1	57.7	6
TB5	2.79	418.52	5	1	1	60.45	6
TB6	3.31	428.38	4	1	1	51.22	6
TB7	1.74	410.45	5	1	1	59.81	6
TB8	1.24	382.48	5	2	1	71.45	10
TB9	0.02	453.55	7	2	1	105.98	8
TB10	1.6	441.52	6	1	1	88.08	5
TB11	1.73	378.43	5	1	1	69.02	4
TB12	1.92	482.63	7	1	1	82.61	7
TB13	2.49	450.56	6	1	1	69.68	6
TB14	1.89	492.64	7	1	1	66.93	8
TB15	1.32	405.52	5	2	1	65.46	6
TB16	2.87	495.55	5	1	1	79.37	8
TB17	1.7	452.56	7	1	1	103.16	5
TB18	1.07	448.59	6	2	1	68.7	7
TB19	1.65	434.51	6	2	1	96.36	9
TB20	1.93	437.56	6	1	1	63.69	9
TB21	0.77	392.48	5	2	1	88.32	5
TB22	1.73	493.61	7	1	1	97.19	7
TB23	2.9	424.52	3	1	1	41.99	5

	9						
TB24	2.23	461.59	5	1	1	71.53	6
TB25	2	436.49	5	1	1	59.81	5
Trimethoprim	-0.41	290.32	7	2	1	105.51	10

Mol. Wt.: Molecular weight; HBA: Hydrogen bond acceptors; HBD: Hydrogen bond donors; TPSA: Total polar surface area.

***In-silico* ADME properties**

Table 3 summarizes summary pharmacokinetic profiles including absorption, distribution, metabolism and elimination of twenty five derivatives and of trimethoprim. Absorption through gastrointestinal tract has been predicted to occur at high levels by all but one compound, namely TB23; the presence of spiro [3.3] heptane and difluoromethyl groups raises its calculated lipophilicity such that absorption is predicted to be low. Of eleven derivatives (TB1, TB4, TB5, TB6, TB7, TB8, TB11, TB14, TB15, TB18 and TB20) permeability to blood brain barrier has been indicated; none of the other fourteen show this property which is preferred for agents targeting peripheral bacterial targets. Eight compounds (TB3, TB9, TB12, TB14, TB17, TB18, TB19 and TB22) have been identified as substrates of P glycoproteins and therefore expected to display some efflux; among seventeen others no substrate status has been confirmed and these should be less susceptible to efflux mediated resistance. Metabolic profiles are uniform throughout the series: each derivative is predicted to inhibit CYP1A2, CYP2C9 and CYP3A4; inhibitors of CYP2D6 have been identified by six compounds (TB4, TB12, TB14, TB16, TB18 and TB22); inhibitors of CYP2C19 have been identified by three compounds (TB14, TB18 and TB22). Permeation coefficients for skin vary between negative values ranging from −0.28 cm/s (for TB23) to −3.08 cm/s (for TB17) according to expectation with higher polarity bearing sulfonylamides and sulfonamides tending toward lower permeation. Scores of abbreviated bio availability are favorable for nineteen compounds and scores of 0.85 have been assigned; the remaining six compounds (TB8, TB9, TB14, TB16, TB19 and TB20) receive score of 0.55 corresponding to that obtained for trimethoprim.

Table 3: Pharmacokinetics and Drug-likeness Properties of All Compounds

Compound Name	GI abs.	BBB pen.	P-gp sub.	CYP1A2 inhibitor	CYP2C19 inhibitor	CYP2C9 inhibitor	CYP2D6 inhibitor	CYP3A4 inhibitor	Log Kp (skin permeation, cm/s)	Ghose	Egan	Muegge	Bioavailability Score
TB1	High	Yes	No	Yes	No	Yes	No	Yes	-1.78	No	No	No	0.85
TB2	High	No	No	Yes	No	Yes	No	Yes	-1.7	No	No	No	0.85
TB3	High	No	Yes	Yes	No	Yes	No	Yes	-3.06	No	No	No	0.85
TB4	High	Yes	No	Yes	No	Yes	Yes	Yes	-2.57	No	No	No	0.85
TB5	High	Yes	No	Yes	No	Yes	No	Yes	-1.78	No	No	No	0.85
TB6	High	Yes	No	Yes	No	Yes	No	Yes	-1.22	No	No	No	0.85
TB7	High	Yes	No	Yes	No	Yes	No	Yes	-1.37	No	No	No	0.85
TB8	High	Yes	No	Yes	No	Yes	No	Yes	-1.88	No	No	No	0.55
TB9	High	No	Yes	Yes	No	Yes	No	Yes	-2.75	No	No	No	0.55
TB10	High	No	No	Yes	No	Yes	No	Yes	-2.29	No	No	No	0.85
TB11	High	Yes	No	Yes	No	Yes	No	Yes	-1.97	No	No	No	0.85
TB12	High	No	Yes	Yes	No	Yes	Yes	Yes	-2.98	No	No	No	0.85
TB13	High	No	No	Yes	No	Yes	No	Yes	-1.81	No	No	No	0.85
TB14	High	Yes	Yes	Yes	Yes	Yes	Yes	Yes	-2.35	No	No	No	0.55
TB15	High	Yes	No	Yes	No	Yes	No	Yes	-1.97	No	No	No	0.85
TB16	High	No	No	Yes	No	Yes	Yes	Yes	-2.24	No	No	No	0.55
TB17	High	No	Yes	Yes	No	Yes	No	Yes	-3.08	No	No	No	0.85
TB18	High	Yes	Yes	Yes	Yes	Yes	Yes	Yes	-2.56	No	No	No	0.85
TB19	High	No	Yes	Yes	No	Yes	No	Yes	-2.63	No	No	No	0.55
TB20	High	Yes	No	Yes	No	Yes	No	Yes	-1.76	No	No	No	0.55
TB21	High	No	No	Yes	No	Yes	No	Yes	-2.42	No	No	No	0.85
TB22	High	No	Yes	Yes	Yes	Yes	Yes	Yes	-2.69	No	No	No	0.85
TB23	Low	No	No	Yes	No	Yes	No	Yes	-0.28	No	No	No	0.85
TB24	High	No	No	Yes	No	Yes	No	Yes	-1.85	No	No	No	0.85
TB25	High	No	No	Yes	No	Yes	No	Yes	-1.27	No	No	No	0.85
Trimethoprim	High	No	No	Yes	No	Yes	No	Yes	-3.58	No	No	No	0.55

GI abs.: Gastrointestinal absorption; BBB pen.: Blood brain barrier permeant; P-gp sub.: P-glycoprotein substrate

In-Silico Toxicity analysis

A predicted toxicity profile is presented for twenty-five derivatives generated using Geintox II. Toxicological classification of twenty compounds according to Globally Harmonized System (GHS) falls into Class 4 because of harmful effects upon oral ingestion. Median Lethal Dose (LD50) ranged from 377.7 to 598.6 mg/kg and highest return was observed for TB9. Remaining five compounds including TB6, TB8, TB11, TB16 and TB21 fall into Class 3 having LD50 ranging from 267.4 to 300.0 mg/kg. Amongst them TB6 stands out as most acute toxic compound. By way of comparison trimethoprim yields an LD50 of 1054.6 mg/kg and therefore the derivatives are predicted to exhibit higher acute toxicity compared to reference standards yet retaining tolerance levels typical for lead candidates currently under development. For all derivatives across the entire series carcinogenesis, mutagenesis, cytotoxicty and immunotoxicity are reported as inactive along with consistently low probabilities. Likewise neither neurotoxicity nor nephrotoxicity nor cardiovascular toxicity have been identified as active. Only three derivatives namely TB5, TB13 and TB20 predict hepatic toxicity with probability of 0.56 but otherwise such calls remain inactive with probabilities varying between 0.15 and 0.32. Members bearing positive predictions for hepatic toxicity share high content of ethers alongside relatively high lipophilicity and such structural features are known drivers of alerts related to liver toxicity.

Table 4: Predicted toxicity of novel substituted thiazole derivatives

Comp. Codes	LD50 (mg/kg)	Toxicity Class	Hepatotoxicity (Prob.)	Carcinogenicity (Prob.)	Immunotoxicity (Prob.)	Mutagenicity (Prob.)	Cytotoxicity (Prob.)
TB1	377.7	4	I (0.27)	I (0.25)	I (0.10)	I (0.12)	I (0.12)
TB2	533.5	4	I (0.29)	I (0.25)	I (0.10)	I (0.12)	I (0.12)
TB3	377.7	4	I (0.21)	I (0.25)	I (0.10)	I (0.12)	I (0.12)
TB4	377.7	4	I (0.24)	I (0.25)	I (0.10)	I (0.12)	I (0.12)
TB5	377.7	4	A (0.56)	I (0.25)	I (0.10)	I (0.12)	I (0.12)
TB6	267.4	3	I (0.31)	I (0.25)	I (0.30)	I (0.12)	I (0.12)
TB7	533.5	4	I (0.30)	I (0.25)	I (0.10)	I (0.12)	I (0.12)
TB8	300.0	3	I (0.18)	I (0.25)	I (0.10)	I (0.12)	I (0.12)
TB9	598.6	4	I (0.23)	I (0.25)	I (0.10)	I (0.12)	I (0.12)
TB10	377.7	4	I (0.25)	I (0.25)	I (0.10)	I (0.12)	I (0.12)
TB11	300.0	3	I (0.17)	I (0.25)	I (0.10)	I (0.12)	I (0.12)
TB12	377.7	4	I (0.23)	I (0.25)	I (0.10)	I (0.12)	I (0.12)
TB13	533.5	4	A (0.56)	I (0.25)	I (0.10)	I (0.12)	I (0.12)
TB14	377.7	4	I (0.27)	I (0.25)	I (0.10)	I (0.12)	I (0.12)
TB15	377.7	4	I (0.26)	I (0.25)	I (0.10)	I (0.12)	I (0.12)
TB16	300.0	3	I (0.28)	I (0.25)	I (0.30)	I (0.12)	I (0.12)
TB17	475.5	4	I (0.21)	I (0.25)	I (0.10)	I (0.12)	I (0.12)
TB18	377.7	4	I (0.24)	I (0.25)	I (0.10)	I (0.12)	I (0.12)
TB19	475.5	4	I (0.23)	I (0.25)	I (0.10)	I (0.12)	I (0.12)
TB20	533.5	4	A (0.56)	I (0.25)	I (0.10)	I (0.12)	I (0.12)
TB21	300.0	3	I (0.15)	I (0.25)	I (0.10)	I (0.12)	I (0.12)
TB22	475.5	4	I (0.25)	I (0.25)	I (0.10)	I (0.12)	I (0.12)
TB23	533.5	4	I (0.32)	I (0.25)	I (0.10)	I (0.12)	I (0.12)
TB24	533.5	4	I (0.29)	I (0.25)	I (0.10)	I (0.12)	I (0.12)
TB25	533.5	4	I (0.31)	I (0.25)	I (0.10)	I (0.12)	I (0.12)
Trimethoprim	1054.6	4	I (0.12)	I (0.10)	I (0.10)	I (0.12)	I (0.12)

A = Active; I = Inactive

Multiparametric selection of lead candidates

Because each compound in the series scored higher than trimethoprim by means of docking calculations affinity alone did not suffice to distinguish these compounds; therefore a sequential filter incorporating binding affinity together with predicted absorption and safety data was used. Compounds scoring at least minus nine point zero kcal/mol on docking were advanced initially. Requirement for high absorption eliminated TB23 because its predicted absorption level was low. Requirement for assignment to GHS toxicity class 4 eliminated TB11 which was the only one of this subset assigned to toxicity class three. Elimination of active hepatotoxicity calls also resulted in elimination of TB13 and requirement of favorable availability score of 0.85 led to exclusion of TB14

since this substance is also a substrate of P glycoproteins and possesses broadest inhibitors of cytochrome P450 within the series. Ultimately elimination of absence of Brenk structural alerts resulted in exclusion of TB2 whose methyl phosphonate moiety bears such an alert. Nine derivatives passed through the complete sequence of filtering steps: TB4, TB7, TB10, TB12, TB17, TB18, TB22, TB24 and TB25. These nine combine affinity scores ranging from minus nine point one two zero to minus nine point six seven two kcal/mol along with high absorption levels, grade 4 acute toxicity, lack of active hepatotoxicity and brief score of 0.85 and free from Brenk alerts and hence were consequently chosen as lead candidates. Among those top scorers among this selection namely TB10, TB22, TB4 and TB24 were then further analyzed for interactions.

Validation of docking protocol

Prior to docking of designed compounds, validation was performed through redocking of co crystallized diaminopyrimidine ligand into the site of Dihydrofolate Reductase (DHFR; PDB ID: 2 W9H) using five distinct grid configurations independently. For each of these configurations all five reproductions exhibited correct experimental binding modes reporting corrected root mean square deviation values ranging from 1.396 to 1.592 Å relative to a threshold level of 2.00 Å and the best configuration reported an RMSD value of 1.396 Å together with docking score of minus 12.190 kcal mol^{-1}. Superposition of the crystallographic pose in green onto poses obtained through subsequent docking reveals good spatial agreement throughout the head group of diaminopyrimidine and trimethyl phenyl ring (Figure 2). This confirms that definitions of grids and scoring functions reproduce observed binding geometries and that the protocol is appropriate for testing compounds.

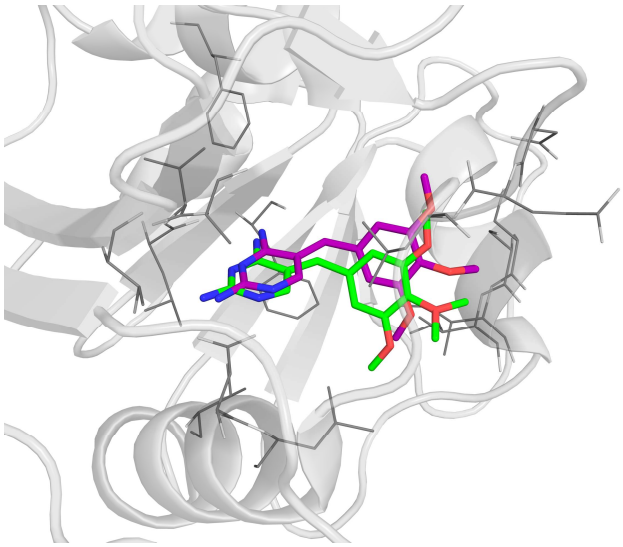

Figure 2: Superimposition of the co-crystallized ligand (green) and the re-docked pose (purple) within the active site of Staphylococcus aureus DHFR (PDB ID: 2 W9H) demonstrating docking protocol validation; RMSD = 1.396 Å.

Results of Molecular Docking

Docking results are reported here for all twenty five thiazoles (TB1 to TB25) against DHFR from Staphylococcus aureus (PDB ID: 2 W9H) along with results for the reference compound trimethoprim. All compounds bind deeper into the folic acid cavity compared to trimethoprim whose highest scoring pose scores −6.730 kcal/mol. The series range from −8.215 kcal/mol to −9.715 kcal/mol; improvements ranging between 1.5 to 3.0 kcal/mol relative to the reference. Amongst the nine preferred lead compounds rankings were TB10 (score −9.672 kcal/mol), TB22 (score −9.586 kcal/mol), TB4 (score −9.433 kcal/mol), TB24 (score −9.377 kcal/mol), TB18 (score −9.307 kcal/mol), TB12 (score −9.295 kcal/mol), TB25 (score −9.294 kcal/mol), TB7 (score −9.175 kcal/mol) and TB17 (score −9.120 kcal/mol). Analysis of profiles of high ranked poses reveals consistent engagement of cavity residues. THR46, LYS45 and PHE92 contact most frequently followed by LEU20, ILE50, ILE14, ASN18, LEU28, VAL31 and ALA7 and GLN95 engage regularly. Compound TB10 forms largest network among members of the series comprising five conventional hydrogen bonds to THR121, THR46, GLN95 and ARG57 with distances of 2.80 Å, 3.13 Å, 3.15 Å and 3.17 and 3.19 Å respectively and two weaker contacts involving PHE92 and LEU28 and nine hydrophobic contacts lining the channel defined by residues such as ILE50, LEU54, VAL31, LEU28, LEU20 and PHE92. Compounds TB22 combine short hydrogen bonding to THR46 with four weak hydrogen bonds and π stack interactions with PHE92 at distance of

5.05 Å; latter contribution is due to 1 methyl imidazole ring. Binding of TB4 and TB24 is largely via shape complementarity with TB4 forming weak hydrogen bonds to ASN18, PHE92 and THR46 and eight hydrophobic contacts whereas TB24 anchors by weak hydrogen bond to PHE92 and extends hydrophobic contacts to residues including ALA7, LYS45, THR121 and GLN95. In comparison, binding of trimethoprim occurs through characteristic signatures of classical anti folates namely salt bridges and hydrogen bonds involving ASP27 and hydrogen bond to LEU20 and engages only six residues altogether resulting in marked difference in score.

Table 5: Molecular docking interaction analysis of novel substituted thiazole derivatives (TB1–TB25) against Staphylococcus aureus DHFR (PDB ID: 2 W9H) with trimethoprim as reference standard.

Compound	Active Amino Residues	Bond Lengths (Å)	Bond Categories	Docking Score (kcal/mol)
TB1	THR121, GLN95, LYS45, ILE14, PHE92, THR121, LYS45, LEU20, VAL31, ALA7, THR46	2.90, 2.97, 5.27, 3.51, 3.53, 3.64, 3.65, 3.75, 3.94, 4.19, 4.19	Hydrogen Bond, Electrostatic, Hydrophobic	−8.489
TB2	THR96, THR96, GLN95, LYS45, LEU54, LYS45, THR46, THR121, MET42, LEU20, PHE92, ILE50, LEU28	2.58, 2.65, 3.24, 5.99, 3.53, 3.62, 3.64, 3.79, 4.03, 4.05, 4.07, 4.25, 4.27	Hydrogen Bond, Electrostatic, Hydrophobic	−9.027
TB3	THR46, ALA7, ASN18, ASP120, LYS45, THR121, LEU20, PHE92, VAL31, LYS45, VAL6, ILE14, PHE98, LEU28	2.97, 3.00, 3.41, 3.80, 5.01, 3.42, 3.50, 3.66, 3.74, 3.76, 4.03, 4.04, 4.20, 4.39	Hydrogen Bond, Electrostatic, Hydrophobic	−8.888
TB4	ASN18, PHE92, THR46, VAL31, LEU28, LEU20, PHE92, LEU54, LYS32, ILE50, THR46, ILE50	3.51, 3.52, 3.54, 3.51, 3.55, 3.56, 3.56, 3.58, 3.65, 3.98, 4.47, 2.23	Hydrogen Bond, Hydrophobic, Unfavourable	−9.433
TB5	ALA7, ASP27, THR96, LYS45, THR121, GLN95, LEU20, ALA7, ILE14, THR96	3.45, 3.71, 2.84, 3.32, 3.51, 3.59, 3.64, 3.85, 3.87, 2.84	Hydrogen Bond, Hydrophobic, Unfavourable	−8.871
TB6	ALA7, THR121, ILE14, THR121, ASN18, LYS45, LYS45, ALA7, PHE92, VAL31, LEU5, ILE14, THR121, THR46, LEU20	3.01, 3.03, 3.55, 3.78, 3.78, 5.80, 3.28, 3.43, 3.45, 3.67, 3.74, 3.76, 3.87, 4.04, 4.41	Hydrogen Bond, Electrostatic, Hydrophobic	−8.649
TB7	THR46, ASP27, ASN18, LEU5, LEU20, LYS45, THR121, ILE14, PHE98, GLN95, VAL6, ALA7	2.85, 3.13, 3.48, 3.71, 3.42, 3.49, 3.55, 3.72, 4.00, 4.21, 4.24, 4.41	Hydrogen Bond, Hydrophobic	−9.175
TB8	ALA7, ASN18, THR46, THR121, VAL31, PHE92, LYS45, LEU20, ALA7, THR46, LEU28, ILE14, LEU5	3.28, 3.44, 3.78, 3.42, 3.47, 3.52, 3.55, 3.62, 3.93, 4.20, 4.21, 4.23, 4.47	Hydrogen Bond, Hydrophobic	−8.215
TB9	GLN95, THR121, THR46, GLY15, ASN18, ASN59, LYS45, THR96, LYS45, LEU20, THR121, THR46, GLN95, ASN18, SER49, THR96	2.95, 3.19, 3.20, 3.20, 3.55, 3.58, 5.41, 2.81, 3.62, 3.77, 3.82, 3.84, 3.93, 4.38, 2.63, 2.81	Hydrogen Bond, Electrostatic, Hydrophobic, Unfavourable	−8.937
TB10	THR121, THR46, GLN95, ARG57, ARG57, PHE92, LEU28, ILE50, LEU54, VAL31, LEU28, THR46, PHE92, LEU20, LYS32, THR121, ILE50, ILE50, ILE50, ILE50	2.80, 3.13, 3.15, 3.17, 3.19, 3.48, 3.75, 2.22, 3.21, 3.27, 3.61, 3.72, 3.85, 4.14, 4.23, 4.44, 2.04, 2.22, 2.51, 2.66	Hydrogen Bond, Hydrophobic, Unfavourable	−9.672
TB11	ALA7, THR121, ASN18, ILE14, ASN18, LEU28, VAL31, THR121, LYS45, LEU20, PHE92, ILE14, THR46, ILE50, ASN18	3.18, 3.27, 3.45, 3.52, 3.70, 3.40, 3.43, 3.57, 3.68, 3.84, 3.89, 3.93, 4.31, 4.48, 4.48	Hydrogen Bond, Hydrophobic	−9.237
TB12	THR46, PHE92, PRO25, LEU28, PHE92, PHE92, LEU54, VAL31, LEU28, LEU20, THR46, ILE14, PHE98, VAL6, LYS32, ILE50, ILE50	2.91, 3.13, 3.40, 3.63, 5.02, 3.41, 3.53, 3.56, 3.57, 3.62, 3.69, 3.73, 3.82, 3.96, 4.09, 4.42, 2.33	Hydrogen Bond, Hydrophobic, Unfavourable	−9.295
TB13	THR121, THR46, LEU28, VAL31, PHE92, LEU54, LYS45, LEU20, THR121, ILE50	2.79, 3.31, 2.94, 3.50, 3.64, 3.68, 3.71, 3.78, 4.19, 4.21	Hydrogen Bond, Hydrophobic	−9.433
TB14	ASN18, ASP27, THR96, ASP120, ILE14, LEU20,	3.27, 3.36, 3.53, 3.55, 3.58, 3.52, 3.57, 3.59,	Hydrogen Bond, Hydrophobic	−9.397

	LYS45, PHE92, THR46, LEU28, THR121, ILE50, VAL31, GLN95	3.67, 3.68, 3.68, 3.83, 3.97, 4.33		
TB15	ASN18, ASN18, LYS45, LYS45, THR46, THR121, LEU54, PHE92, MET42, GLN95	3.54, 3.64, 5.65, 3.58, 3.59, 3.69, 3.71, 3.75, 3.78, 4.41	Hydrogen Bond, Electrostatic, Hydrophobic	−8.734
TB16	THR121, GLN95, LYS45, VAL31, PHE92, LYS45, THR121, LEU28, ILE14, LEU20, THR46, ILE50, ALA7	2.89, 3.07, 5.34, 3.26, 3.28, 3.69, 3.70, 3.76, 3.77, 3.89, 4.04, 4.08, 4.23	Hydrogen Bond, Electrostatic, Hydrophobic	−8.837
TB17	THR46, LYS29, THR46, PHE92, LEU28, LEU54, LYS32, LEU28, VAL31, ILE14, PHE92, LEU20, ILE50, THR46, THR121, ILE50	2.90, 3.34, 3.21, 3.51, 3.59, 3.47, 3.50, 3.60, 3.60, 3.84, 3.91, 3.95, 3.98, 4.05, 4.36, 2.55	Hydrogen Bond, Hydrophobic, Unfavourable	−9.120
TB18	THR46, PHE92, VAL31, PHE92, LEU28, ILE14, LEU54, LYS32, LEU20, ILE50, THR121, THR46, ILE50	3.06, 3.53, 3.42, 3.43, 3.51, 3.60, 3.70, 3.70, 3.77, 3.99, 4.17, 4.45, 2.36	Hydrogen Bond, Hydrophobic, Unfavourable	−9.307
TB19	THR46, THR46, ASN18, ASP120, ASN18, LYS45, LYS45, THR46, THR121, GLN95, PHE92, MET42, LEU54, ASN18, SER49, SER49	2.79, 3.10, 3.23, 3.57, 3.74, 5.56, 3.72, 3.73, 3.73, 3.80, 4.05, 4.07, 4.10, 4.48, 2.25, 2.51	Hydrogen Bond, Electrostatic, Hydrophobic, Unfavourable	−8.439
TB20	THR46, ALA7, ASP27, GLN95, LYS45, ILE14, VAL6, THR96, THR121, LEU20, LYS45, PHE98, GLN95	2.99, 3.10, 3.35, 3.42, 5.29, 3.44, 3.52, 3.53, 3.61, 3.62, 3.70, 3.76, 4.08	Hydrogen Bond, Electrostatic, Hydrophobic	−8.955
TB21	THR46, ALA7, THR121, ASN18, ASN18, LYS45, LYS45, THR121, LEU20, ALA7, LYS45, ILE14, ASN18, VAL6	2.98, 3.12, 3.57, 3.65, 3.69, 4.61, 5.14, 3.41, 3.73, 3.85, 4.05, 4.15, 4.19, 4.45	Hydrogen Bond, Electrostatic, Hydrophobic	−8.919
TB22	THR46, PHE92, THR46, ILE14, LEU28, PHE92, LEU54, PHE92, LEU28, VAL31, LEU20, THR46, LYS32, ILE50, ILE50	2.76, 3.22, 3.37, 3.54, 3.72, 5.05, 3.44, 3.48, 3.59, 3.59, 3.62, 3.84, 3.85, 4.35, 2.27	Hydrogen Bond, Hydrophobic, Unfavourable	−9.586
TB23	THR121, GLN95, LYS45, VAL31, LEU20, ALA7, PHE92, THR46, THR121, LYS45, LEU28, ILE50, LEU5, ILE14	3.06, 3.17, 5.23, 3.34, 3.36, 3.53, 3.58, 3.59, 3.63, 3.71, 3.78, 3.89, 3.90, 3.91	Hydrogen Bond, Electrostatic, Hydrophobic	−9.715
TB24	PHE92, THR121, LEU20, LYS45, GLN95, PHE92, ALA7, VAL31, ILE14, ILE50	3.76, 3.59, 3.59, 3.59, 3.67, 3.83, 3.86, 3.91, 4.34, 4.36	Hydrogen Bond, Hydrophobic	−9.377
TB25	THR46, ILE14, ASN18, THR121, LYS45, VAL31, THR121, LEU20, PHE98, VAL6, LYS45, ILE14, ALA7, ASN18	2.83, 3.04, 3.41, 3.69, 4.84, 3.44, 3.48, 3.55, 3.62, 3.76, 3.79, 3.79, 3.97, 4.26	Hydrogen Bond, Electrostatic, Hydrophobic	−9.294
Trimethoprim	ASP27, LEU20, SER49, ASN18, PHE92, ASN18, ASP27, PHE92, LEU20, THR46, SER49	3.18, 3.34, 2.27, 3.72, 3.75, 3.75, 4.00, 3.72, 3.92, 4.03, 2.27	Hydrogen Bond, Electrostatic, Hydrophobic, Unfavourable	−6.730

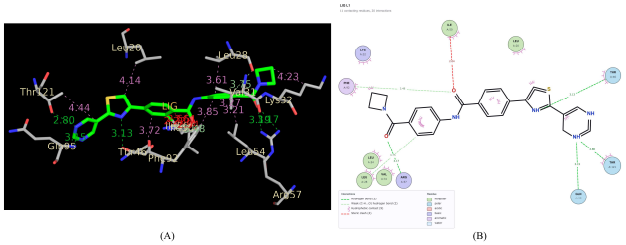

Figure 3: Molecular docking interaction plots of TB10 with Staphylococcus aureus DHFR (PDB ID: 2 W9H); (A) 3D interaction plot and (B) 2D interaction plot.

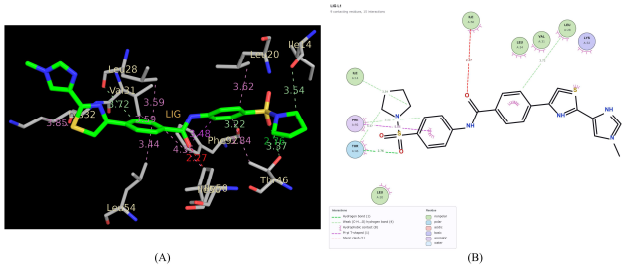

Figure 4: Molecular docking interaction plots of TB22 with Staphylococcus aureus DHFR (PDB ID: 2 W9H); (A) 3D interaction plot and (B) 2D interaction plot.

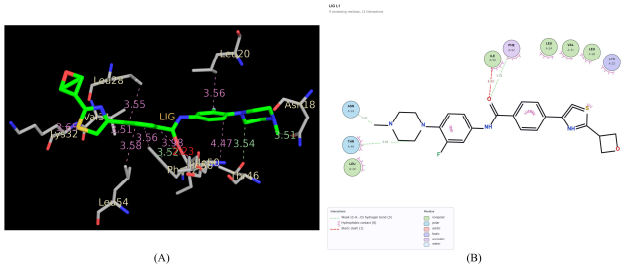

Figure 5: Molecular docking interaction plots of TB4 with Staphylococcus aureus DHFR (PDB ID: 2 W9H); (A) 3D interaction plot and (B) 2D interaction plot.

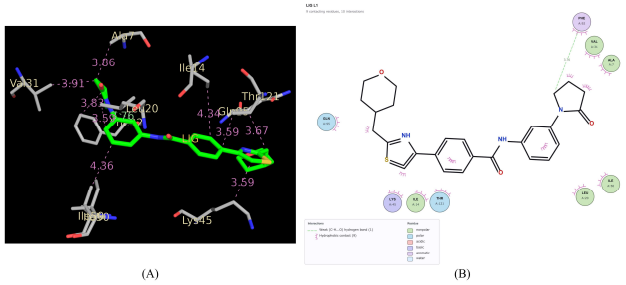

Figure 6: Molecular docking interaction plots of TB24 with Staphylococcus aureus DHFR (PDB ID: 2 W9H); (A) 3D interaction plot and (B) 2D interaction plot.

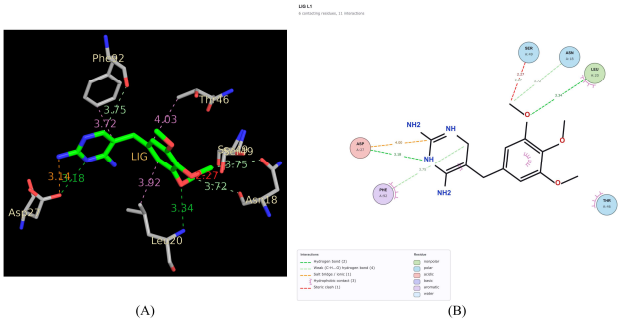

(A) (B)

Figure 7: Molecular docking interaction plots of trimethoprim (reference standard) with Staphylococcus aureus DHFR (PDB ID: 2 W9H); (A) 3D interaction plot and (B) 2D interaction plot.

Discussion

Assessment of drug likeness demonstrates achievement of the intended aim through decoupling of substituent at carbon atom number two of thiazole away from substitution at anilide. Earlier series constructed upon this scaffold have previously assigned tert butyl substituent at site number two; properties in these compounds were largely defined by substituent aniline ring, which drove them toward high lipophilicity [36, 37]. By sourcing substituent number 2 from carboxythio amide, various oxetanyl, oxolan, oxane, azetidinyl, piperazino, morpholino and pyrimido functional groups may be introduced into such positions and effects are evident in Table 2. Thus M Log P varies greatly exceeding three log units whereas molecular weight remains less than 500 g mol^{-1} and polar surface area under 106 $Å^2$ [38, 39]. Single violations noted for each compound relate to lipophilicity terms and not breaches relating to size or hydrogen bonding; therefore comparative series lacks penalty related to drug likeness relative to comparator used clinically [40].

The predicted pharmacokinetics profile proves generally favorable for oral administration. Twenty four out of twenty five compounds exhibit high gastrointestinal absorption and lack recognition by substrates of P glycoproteins; such results suggest that scaffolds will achieve systemic levels without immediate return to the gut lumen which is important for antibiotics against which efflux constitutes a mechanism of resistance [41]. Failure of compound TB23 to meet criteria for absorption stands out because it is the sole example containing spiro [3.3] heptane moiety at position 2 along with difluoromethyl aniline; though this combination resulted in highest docking scores among members of the series, resulting lipophilicity conflicts with oral absorption [42]. Among those fourteen compounds expected to fail penetration into blood brain barrier, selection towards peripheral bacterial targets seems desirable as central targeting confers no therapeutic advantage but increases tolerance risk [43]. Consistent liabilities uniformly predicted throughout the series for inhibition of CYP1A2, CYP2C9 and CYP3 A4 appear to result from nature of benzamide core and requires experimental verification prior to designation as real risks for development [44].

Safety assessments based upon toxicity predictions support overall safety of the chemical series. For carcinogenesis, mutagenesis, cytotoxicity and immune toxicity none of the twenty five derivatives showed significant results at low probabilities; thus introduction of thi唑 ring or benzylidene linkage does not introduce alerts regarding genotoxic properties or cytotoxicity [45]. Alert of hepatotoxicity was raised specifically for compounds TB5, TB13 and TB20 and shared features among them include rich oxygen containing and lipophilic ethers substituents on the phenyl ring: oxetanyl oxy substituent in TB5, oxane 4 yl oxy substituent in TB13 and 2 methoxy ethoxy substituent in TB20 [46]. It is important for future design that such alerts track specific substitution patterns rather than limitations inherent within scaffold core [47]. Similarly interpretation is possible also for five class 3 members: TB6, TB8, TB11, TB16 and TB21 exhibit small weak elaborations at either of variable position and lower predicted LD50 values indicate protection from further increase of molecular complexity at such sites [48].

Results of docking studies clearly delineate a relationship between structural features and activity levels. Each of the derivatives surpasses performance of trimethoprim and this becomes apparent upon consideration of profile interactions: Trimethoprim interacts via engagement of only six residues, deriving most binding energy from salt bridge involving residue ASP27; contrastingly, extended thiazole axis penetrates entire length of folic acid channel and contacts nine to fourteen residues [49]. Binding affinity among members correlates directly with extent to which terminal substituent groups achieve specific polar contact. TB10 stands out as particularly prominent exemplar: its 5 position pyrimidine group donates

and accepts hydrogen bonds at residue THR46, THR121 and GLN95 while carbonyl aniline azetidinone moiety contacts ARG57 and gives rise to five conventional hydrogen bonds exceeding those produced by all other members together along with nine hydrophobic contacts [50]. Similarly high ranking is achieved by TB22 using distinct strategies: imidazole ring of TB22 forms π stacking interaction with residue PHEN92 at distance 5.05 Å alongside short hydrogen bond to THR46 [51]. Binding of TB4 and TB24 relies mainly on shape complementarity and scoring below TB10 reflects substitution of weaker C H·· O contacts for conventional hydrogen bonds [52]. General lesson is that nitrogen containing aromatic heterocycles at position 2 perform better compared to ethers of similar size since these moieties serve as acceptors of hydrogen bonding against network of hydroxylic THRE46 and THRE121 [53]. Noteworthy too is absence of involvement of ASP27 interaction relied upon by trimethoprim; derivatives adopt hydrophobic shelf occupied by LEU20, LEU28, VAL31, ILE50, LEU54 and PHEN92 instead [54]. Given clustering of resistant mutations near dipyrimidine recognition site substitutions that do not depend on that interaction stand out as desirable feature for second generation antifolates and this appears to be one of most important findings of this research [55].

Converging through consideration of three distinct predictive layers leads to a consistent result. Selection based solely upon affinity alone would rank TB23, TB10, TB22 and TB13 first [56]. However, TB23 has been predicted to exhibit poor absorption whereas TB13 shows signs of hepatotoxicity; therefore both of these top ranked candidate compounds fail to meet requirements for oral development although they show high binding energies [57]. By means of the previously described sequential filters such undesirable selection is avoided and nine candidates emerge which satisfy simultaneously affinity, absorption and safety standards. Of these, TB10 stands out particularly; notable among its attributes are highest docking scores within the entire series along with high levels of gastrointestinal absorption, absence of liability towards P glycoproteins, lack of penetration into brain tissue, classification of low acute toxicity level, absence of hepatic toxicity and a bioavailability score of 0.85 [58]. Such combined characteristics apart from reliance upon ASP27 contacts used by dipyrimidine analogues also render it an especially promising lead compound. Principal limitations inherent in the current study lie in dependence exclusively upon computational predictions; rankings regarding affinities, calls concerning absorption and alerts related to toxicity each demand experimental verification and close scrutiny of anticipated cytochrome P450 inhibition is required.

Conclusion

Twenty five novel substituted derivatives bearing thiazoles (TB1 to TB25), synthesized using a two stage process wherein substitution at position C2 of thiazole and anilide substituents are varied independently, have been elaborately studied employing FT IR spectroscopy, proton nuclear magnetic resonance (^{1}H NMR), carbon nuclear magnetic resonance (^{13}C NMR) and electrospray ionization mass spectrometry (ESI MS). These compounds have been tested computationally against Staphylococcus aureus dihydrofolate reductase. Each of these fifty compounds complies with both Lipinski's rule and Veber's rule; each exhibits one violation of lipophilicity criterion. Twenty four compounds are predicted to be highly absorbent into gastrointestinal tracts and all show absence of carcinogenicity, mutagenicity, cytotoxicity and immunotoxicity across the series. Docking scores indicate strong affinity compared to trimethoprim ranging from negative eighty point one five to minus nine point seven one five kcal/mol relative to negative six point seven three zero kcal/mol for reference standard. Sequential filters based upon docking score, gastrointestinal absorption profile, Globally Harmonized System of Classification and Labelling of Chemicals (GHS) toxicity class, hepatotoxicity and bio availability score along with structural alerts resulted in identification of nine lead candidates among them TB10, TB22, TB4 and TB24 exhibit highest binding affinity. Binding occurs primarily through a hydroxyl network formed between Thr46 and Thr121 residues and hydrophobic shelf rather than through interaction at Asp27 to which dipyrimidine analogues are dependent. Such binding mode might be less susceptible to resistance attributable substitutions. Amongst the series TB10 stands out as the most promising candidate and further in vitro bacterial screening and assay targeting inhibition of dihydrofolate reductase is warranted to substantiate results reported herein.

Abbreviations

DHFR: Dihydrofolate reductase; FT-IR: Fourier-transform infrared spectroscopy; NMR: Nuclear magnetic resonance; ESI-MS: Electrospray ionization mass spectrometry; ADME: Absorption, distribution, metabolism, and excretion; TPSA: Total polar surface area; MLogP: Moriguchi octanol-water partition coefficient; HBA: Hydrogen bond acceptors; HBD: Hydrogen bond donors; GI: Gastrointestinal; BBB: Blood-brain barrier; P-gp: P-glycoprotein; CYP: Cytochrome P450; LD50: Median lethal dose; GHS: Globally Harmonized System of Classification and Labelling

of Chemicals; QED: Quantitative estimate of drug-likeness; PAINS: Pan-assay interference compounds; RMSD: Root-mean-square deviation; MMFF94: Merck molecular force field 94; PDB: Protein Data Bank; SAR: Structure-activity relationship; DCM: Dichloromethane; DMF: N,N-Dimethylformamide; m.p.: Melting point.

REFERENCES

1. Chamodini, K., Samarasingha, S., Didulanga, K., & Jayasekara, C. (2025). Bioactive Compounds in Natural Remedies and Functional Foods for Managing Recurrent Urinary Tract Infections in Postmenopausal Women. *Journal of Menopausal Medicine*, *31*(3), 145. https://doi.org/10.6118/jmm.25117
2. El-Zawawy, N. A., Ali, S. S., Khalil, M. A., Sun, J., & Nouh, H. S. (2022). Exploring the potential of benzoic acid derived from the endophytic fungus strain Neurospora crassa SSN01 as a promising antimicrobial agent in wound healing. *Microbiological Research*, *262*, 127108. https://doi.org/10.1016/j.micres.2022.127108
3. Nunes, E., Frihling, B., Barros, E., de Oliveira, C., Verbisck, N., Flores, T., … Luna, K. (2020). Antibiofilm Activity of Acidic Phospholipase Isoform Isolated from Bothrops erythromelas Snake Venom. *Toxins*, *12*(9), 606. https://doi.org/10.3390/toxins12090606
4. Singhal, R., Mehra, M. K., Malik, B., & Pilania, M. (2024). Iodine/DMSO-catalyzed oxidative deprotection of *N* -tosylhydrazone for benzoic acid synthesis. *RSC Advances*, *14*(41), 30482–30486. https://doi.org/10.1039/d4ra05849f
5. Rong, R., Zhang, R., Wang, X., Dan, Y., Zhao, Y., & Yu, Z. (2019). Synthesis, pharmacological evaluation and molecular docking of novel R-/S-2-(2-hydroxypropanamido)-5-trifluoromethyl benzoic acid as dual anti-inflammatory anti-platelet aggregation agents. *Naunyn-Schmiedeberg's Archives of Pharmacology*, *393*(6), 967–978. https://doi.org/10.1007/s00210-019-01753-9
6. Rohatgi, A., & Gupta, P. (2023). Benzoic acid derivatives as potent antibiofilm agents against Klebsiella pneumoniae biofilm. *Journal of Bioscience and Bioengineering*, *136*(3), 190–197. https://doi.org/10.1016/j.jbiosc.2023.06.011
7. G, S., Pathoor, N. N., Murthykumar, K., & Ganesh, P. S. (2025). Targeting Pseudomonas aeruginosa PAO1 pathogenicity: The role of Glycyrrhiza glabra in inhibiting virulence factors and biofilms. *Diagnostic Microbiology and Infectious Disease*, *111*(3), 116674. https://doi.org/10.1016/j.diagmicrobio.2024.116674
8. Das, D. N., & Ravi, N. (2022). Influences of polycyclic aromatic hydrocarbon on the epigenome toxicity and its applicability in human health risk assessment. *Environmental Research*, *213*, 113677. https://doi.org/10.1016/j.envres.2022.113677
9. Nwosu, Z. C., Battello, N., Rothley, M., Piorońska, W., Sitek, B., Ebert, M. P., … Dooley, S. (2018). Liver cancer cell lines distinctly mimic the metabolic gene expression pattern of the corresponding human tumours. *Journal of Experimental & Clinical Cancer Research*, *37*(1), 211. https://doi.org/10.1186/s13046-018-0872-6
10. Goldstein, M., & Goodey, N. M. (2020). Distal Regions Regulate Dihydrofolate Reductase-Ligand Interactions. *Methods in Molecular Biology*, *2253*, 185–219. https://doi.org/10.1007/978-1-0716-1154-8_12
11. Arthur, M. N., Hanson, G., Broni, E., Sakyi, P. O., Mensah-Brown, H., Miller, W. A., & Kwofie, S. K. (2024). Natural Product Identification and Molecular Docking Studies of Leishmania Major Pteridine Reductase Inhibitors. *Pharmaceuticals*, *18*(1), 6. https://doi.org/10.3390/ph18010006
12. Huan, C., Xu, Y., Zhang, W., Guo, T., Pan, H., & Gao, S. (2021). Research Progress on the Antiviral Activity of Glycyrrhizin and its Derivatives in Liquorice. *Frontiers in Pharmacology*, *12*, 680674. https://doi.org/10.3389/fphar.2021.680674
13. Davidova, S., Galabov, A. S., & Satchanska, G. (2024). Antibacterial, Antifungal, Antiviral Activity, and Mechanisms of Action of Plant Polyphenols. *Microorganisms*, *12*(12), 2502. https://doi.org/10.3390/microorganisms12122502
14. Khan, Y., Maalik, A., Rehman, W., Alanazi, M. M., Khan, S., Hussain, R., … Iqbal, S. (2024). Synthesis, *in Vitro* Bio-Evaluation and *in Silico* Molecular Docking Studies of Thiadiazole-Based Schiff Base Derivatives. *Future Medicinal Chemistry*, *16*(4), 335–348. https://doi.org/10.4155/fmc-2023-0276
15. Elli, S., Sisto, T., Nizzolo, S., Freato, N., Bertocchi, L., Bianchini, G., … Guerrini, M. (2024). Modeling the Detailed Conformational Effects of the Lactosylation of Hyaluronic Acid. *Biomacromolecules*, *26*(1), 541–555. https://doi.org/10.1021/acs.biomac.4c01318

16. Podila, N., Penddinti, N. K., Rudrapal, M., Rakshit, G., Konidala, S. K., Pulusu, V. S., … Shaik, A. B. (2024). Design, synthesis, biological and computational screening of novel pyridine-based thiadiazole derivatives as prospective anti-inflammatory agents. *Heliyon*, *10*(8), e29390. https://doi.org/10.1016/j.heliyon.2024.e29390
17. Almandil, N. B., Taha, M., Gollapalli, M., Rahim, F., Ibrahim, M., Mosaddik, A., & Anouar, E. H. (2019). Indole bearing thiadiazole analogs: synthesis, β-glucuronidase inhibition and molecular docking study. *BMC Chemistry*, *13*(1), 14. https://doi.org/10.1186/s13065-019-0522-x
18. Rubab, S. L., Raza, A. R., Nisar, B., Ashfaq, M., Altaf, Y., Hussain, R., … Ali, H. M. (2023). Synthesis, Crystal Structure, DFT Calculations, Hirshfeld Surface Analysis and In Silico Drug-Target Profiling of (R)-2-(2-(1,3-Dioxoisoindolin-2-yl)propanamido)benzoic Acid Methyl Ester. *Molecules*, *28*(11), 4375. https://doi.org/10.3390/molecules28114375
19. Collin, F., & Maxwell, A. (2019). The Microbial Toxin Microcin B17: Prospects for the Development of New Antibacterial Agents. *Journal of Molecular Biology*, *431*(18), 3400–3426. https://doi.org/10.1016/j.jmb.2019.05.050
20. Wróbel, A., Arciszewska, K., Maliszewski, D., & Drozdowska, D. (2019). Trimethoprim and other nonclassical antifolates an excellent template for searching modifications of dihydrofolate reductase enzyme inhibitors. *The Journal of Antibiotics*, *73*(1), 5–27. https://doi.org/10.1038/s41429-019-0240-6
21. Zheng, J., & Conrad, M. (2025). Ferroptosis: when metabolism meets cell death. *Physiological Reviews*, *105*(2), 651–706. https://doi.org/10.1152/physrev.00031.2024
22. Rotondi, G., Guglielmi, P., Carradori, S., Secci, D., De Monte, C., De Filippis, B., … Supuran, C. T. (2019). Design, synthesis and biological activity of selective hCAs inhibitors based on 2-(benzylsulfinyl)benzoic acid scaffold. *Journal of Enzyme Inhibition and Medicinal Chemistry*, *34*(1), 1400–1413. https://doi.org/10.1080/14756366.2019.1651315
23. Zhang, X., Wang, Y., Li, X., Wu, J., Zhao, L., Li, W., & Liu, J. (2021). Dynamics-Based Discovery of Novel, Potent Benzoic Acid Derivatives as Orally Bioavailable Selective Estrogen Receptor Degraders for ERα+ Breast Cancer. *Journal of Medicinal Chemistry*, *64*(11), 7575–7595. https://doi.org/10.1021/acs.jmedchem.1c00280
24. Issa, H. M., & Mohammed, D. H. (2025). A critical review on the journey of benzoic acid in the pharmaceutical industry from manufacturing processes through various uses to disposal: An environmental perspective. *Environmental Analysis Health and Toxicology*, *40*(1), e2025007. https://doi.org/10.5620/eaht.2025007
25. Elhrech, H., Aguerd, O., El Kourchi, C., Gallo, M., Naviglio, D., Chamkhi, I., & Bouyahya, A. (2024). Comprehensive Review of Olea europaea: A Holistic Exploration into Its Botanical Marvels, Phytochemical Riches, Therapeutic Potentials, and Safety Profile. *Biomolecules*, *14*(6), 722. https://doi.org/10.3390/biom14060722
26. Tirumala, M. G., Anchi, P., Raja, S., Rachamalla, M., & Godugu, C. (2021). Novel Methods and Approaches for Safety Evaluation of Nanoparticle Formulations: A Focus Towards In Vitro Models and Adverse Outcome Pathways. *Frontiers in Pharmacology*, *12*, 612659. https://doi.org/10.3389/fphar.2021.612659
27. Elmaaty, A. A., Darwish, K. M., Khattab, M., Elhady, S. S., Salah, M., Hamed, M. I. A., … Saleh, M. M. (2021). In a search for potential drug candidates for combating COVID-19: computational study revealed salvianolic acid B as a potential therapeutic targeting 3CLpro and spike proteins. *Journal of Biomolecular Structure and Dynamics*, *40*(19), 8866–8893. https://doi.org/10.1080/07391102.2021.1918256
28. Dawood, M., Elbadawi, M., Böckers, M., Bringmann, G., & Efferth, T. (2020). Molecular docking-based virtual drug screening revealing an oxofluorenyl benzamide and a bromonaphthalene sulfonamido hydroxybenzoic acid as HDAC6 inhibitors with cytotoxicity against leukemia cells. *Biomedicine & Pharmacotherapy*, *129*, 110454. https://doi.org/10.1016/j.biopha.2020.110454
29. Tan, M.-X., Wang, Z.-F., Qin, Q.-P., Zou, B.-Q., & Liang, H. (2020). Complexes of oxoplatin with rhein and ferulic acid ligands as platinum(<scp>iv</scp>) prodrugs with high anti-tumor activity. *Dalton Transactions*, *49*(5), 1613–1619. https://doi.org/10.1039/c9dt04594e
30. Pavlova, A., Lynch, D. L., Daidone, I., Zanetti-Polzi, L., Smith, M. D., Chipot, C., … Gumbart, J. C. (2021). Inhibitor binding influences the protonation states of histidines in SARS-CoV-2 main protease. *Chemical*

Science, *12*(4), 1513–1527. https://doi.org/10.1039/d0sc04942e

31. Cai, X., Haider, K., Lu, J., Radic, S., Son, C. Y., Cui, Q., & Gunner, M. R. (2018). Network analysis of a proposed exit pathway for protons to the P-side of cytochrome c oxidase. *Biochimica et Biophysica Acta (BBA) - Bioenergetics*, *1859*(10), 997–1005. https://doi.org/10.1016/j.bbabio.2018.05.010
32. Nguyen, A.-K., Lerttanakij, P., Taweechat, P., Sompornpisut, P., Khotwong, S., Wacharasindhu, S., & Phuwapraisirisan, P. (2025). α-Glucosidase Inhibitors from the Leaves of *Cannabis sativa*: Structure–Activity Relationship, Kinetic Investigation, and Molecular Docking. *Journal of Agricultural and Food Chemistry*, *73*(33), 20900–20915. https://doi.org/10.1021/acs.jafc.5c08443
33. Escandón-Rivera, S. M., Andrade-Cetto, A., Rosas-Ramírez, D. G., Mata-Torres, G., & Arreguín-Espinosa, R. (2026). Ent–Clerodane Diterpenoid Inhibitors of Glucose-6-phosphatase from Croton guatemalensis Lotsy. *Plants*, *15*(3), 442. https://doi.org/10.3390/plants15030442
34. Vidossich, P., Manathunga, M., Götz, A. W., Merz, K. M., & De Vivo, M. (2025). Aliphatic Polyester Recognition and Reactivity at the Active Cleft of a Fungal Cutinase. *Journal of Chemical Information and Modeling*, *65*(9), 4662–4673. https://doi.org/10.1021/acs.jcim.5c00739
35. Alvarez-Ricardo, Y., Puentes-Díaz, N., Macías, M. A., Alí-Torres, J., & Hurtado, J. J. (2026). New Coordination Polymers with Unexpected Octahedral copper(II) Geometry: Synthesis, Supramolecular and Theoretical Study. *ACS Omega*, *11*(20), 29390–29398. https://doi.org/10.1021/acsomega.5c07364
36. Makhaeva, G. F., Lushchekina, S. V., Boltneva, N. P., Serebryakova, O. G., Kovaleva, N. V., Rudakova, E. V., … Richardson, R. J. (2021). Novel potent bifunctional carboxylesterase inhibitors based on a polyfluoroalkyl-2-imino-1,3-dione scaffold. *European Journal of Medicinal Chemistry*, *218*, 113385. https://doi.org/10.1016/j.ejmech.2021.113385
37. Pflégr, V., Horváth, L., Stolaříková, J., Pál, A., Korduláková, J., Bősze, S., … Krátký, M. (2021). Design and synthesis of 2-(2-isonicotinoylhydrazineylidene)propanamides as InhA inhibitors with high antitubercular activity. *European Journal of Medicinal Chemistry*, *223*, 113668. https://doi.org/10.1016/j.ejmech.2021.113668
38. Araya-Hermosilla, E., Catalán-Toledo, J., Muñoz-Suescun, F., Oyarzun-Ampuero, F., Raffa, P., Polgar, L. M., … Moreno-Villoslada, I. (2018). Totally Organic Redox-Active pH-Sensitive Nanoparticles Stabilized by Amphiphilic Aromatic Polyketones. *The Journal of Physical Chemistry B*, *122*(5), 1747–1755. https://doi.org/10.1021/acs.jpcb.7b11254
39. Delmas, W. G., Vickers, E. T., DiBenedetto, A. C., Lum, C., Hernandez, I. N., Zhang, J. Z., & Ghosh, S. (2020). Modulating Charge Carrier Dynamics and Transfer via Surface Modifications in Organometallic Halide Perovskite Quantum Dots. *The Journal of Physical Chemistry Letters*, *11*(18), 7886–7892. https://doi.org/10.1021/acs.jpclett.0c02151
40. Li, H., Xu, T., Peng, Q., Chen, Y., Zhou, H., Lu, Y., & Yan, R. (2021). Enzymatic acylation of rutin with benzoic acid ester and lipophilic, antiradical, and antiproliferative properties of the acylated derivatives. *Journal of Food Science*, *86*(5), 1714–1725. https://doi.org/10.1111/1750-3841.15703
41. Veneranda, M., Lopez-Reyes, G., Manrique, J. A., Medina, J., Ruiz-Galende, P., Torre-Fdez, I., … Rull, F. (2020). ExoMars Raman Laser Spectrometer: A Tool for the Potential Recognition of Wet-Target Craters on Mars. *Astrobiology*, *20*(3), 349–363. https://doi.org/10.1089/ast.2019.2095
42. Eliaa, S. G., Al-Karmalawy, A. A., Saleh, R. M., & Elshal, M. F. (2020). Empagliflozin and Doxorubicin Synergistically Inhibit the Survival of Triple-Negative Breast Cancer Cells via Interfering with the mTOR Pathway and Inhibition of Calmodulin: *In Vitro* and Molecular Docking Studies. *ACS Pharmacology & Translational Science*, *3*(6), 1330–1338. https://doi.org/10.1021/acsptsci.0c00144
43. Jacobs, M. R., Olivero, J. E., Ok Choi, H., Liao, C.-P., Kashemirov, B. A., Katz, J. E., … McKenna, C. E. (2023). Synthesis and anti-cancer potential of potent peripheral MAOA inhibitors designed to limit blood:brain penetration. *Bioorganic & Medicinal Chemistry*, *92*, 117425. https://doi.org/10.1016/j.bmc.2023.117425
44. Peng, T., Xu, C., Yang, L., Yang, B., Cai, W.-W., Gu, F., & Ying, G.-G. (2022). Kinetics and Mechanism of Degradation of Reactive Radical-Mediated Probe Compounds by the UV/Chlorine Process: Theoretical Calculation and Experimental Verification. *ACS Omega*, *7*(6), 5053–5063. https://doi.org/10.1021/acsomega.1c06001
45. Yong, Y. F., Liu, S., Sakai, K., Fujiyama, K., Takagi, H., Futamura, Y., … Takahashi, S.

(2025). Biosynthesis of reveromycin derivatives by altering the regioselectivity of cytochrome P450revI. *Chemical Science*, *16*(28), 13106–13114. https://doi.org/10.1039/d5sc01355k

46. Yi, S., Chen, P., Yang, L., & Zhu, L. (2019). Probing the hepatotoxicity mechanisms of novel chlorinated polyfluoroalkyl sulfonates to zebrafish larvae: Implication of structural specificity. *Environment International*, *133*(Pt B), 105262. https://doi.org/10.1016/j.envint.2019.105262
47. Zenchenko, A. A., Kaleda, M. K., Uvarova, V. I., Khvatov, E. V., Osolodkin, D. I., & Oslovsky, V. E. (2026). Design of Nucleoside Prodrugs for the Inhibition of Tick-Borne Encephalitis Virus Reproduction. *Doklady Biochemistry and Biophysics*. https://doi.org/10.1134/s1607672926600156
48. Kim, M. S., Lee, C., & Kim, J.-H. (2021). Occurrence of unknown reactive species in UV/H2O2 system leading to false interpretation of hydroxyl radical probe reactions. *Water Research*, *201*, 117338. https://doi.org/10.1016/j.watres.2021.117338
49. Agili, F. (2024). Novel Thiazole Derivatives Containing Imidazole and Furan Scaffold: Design, Synthesis, Molecular Docking, Antibacterial, and Antioxidant Evaluation. *Molecules*, *29*(7), 1491. https://doi.org/10.3390/molecules29071491
50. Phua, S. Z. F., Yang, G., Lim, W. Q., Verma, A., Chen, H., Thanabalu, T., & Zhao, Y. (2019). Catalase-Integrated Hyaluronic Acid as Nanocarriers for Enhanced Photodynamic Therapy in Solid Tumor. *ACS Nano*, *13*(4), 4742–4751. https://doi.org/10.1021/acsnano.9b01087
51. Xiao, T., Wei, Y., Cui, M., Li, X., Ruan, H., Zhang, L., … Zhou, H. (2021). Effect of dihydromyricetin on SARS-CoV-2 viral replication and pulmonary inflammation and fibrosis. *Phytomedicine*, *91*, 153704. https://doi.org/10.1016/j.phymed.2021.153704
52. Sánchez-González, Á., Grenut, P., & Gil, A. (2022). Influence of conventional hydrogen bonds in the intercalation of phenanthroline derivatives with DNA: The important role of the sugar and phosphate backbone. *Journal of Computational Chemistry*, *43*(11), 804–821. https://doi.org/10.1002/jcc.26836
53. Hagar, M., Ahmed, H. A., Aljohani, G., & Alhaddad, O. A. (2020). Investigation of Some Antiviral N-Heterocycles as COVID 19 Drug: Molecular Docking and DFT Calculations. *International Journal of Molecular Sciences*, *21*(11), 3922. https://doi.org/10.3390/ijms21113922
54. Drozdowska, D., Wróbel-Tałałaj, A., Parzych, C., & Ratkiewicz, A. (2024). Benzamide Trimethoprim Derivatives as Human Dihydrofolate Reductase Inhibitors—Molecular Modeling and In Vitro Activity Study. *Biomedicines*, *12*(5), 1079. https://doi.org/10.3390/biomedicines12051079
55. Gao, X., Wu, M., Zhang, W., Li, C., Guo, R.-T., Dai, Y., … Qin, H.-M. (2021). Structural Basis of Salicylic Acid Decarboxylase Reveals a Unique Substrate Recognition Mode and Access Channel. *Journal of Agricultural and Food Chemistry*, *69*(39), 11616–11625. https://doi.org/10.1021/acs.jafc.1c04091
56. Yin, X., Wang, S., Wang, Z., Wen, H., Bai, T., & Zhang, Y. (2024). Effects of Pretreatment Methods on Gamma-Aminobutyric Acid Enrichment and Quality Improvement in Highland Barley Beverages. *Foods*, *13*(24), 4053. https://doi.org/10.3390/foods13244053
57. Santos, S. J. M., & Valentini, A. (2024). In silico investigation of Komaroviquinone as a potential inhibitor of SARS-CoV-2 main protease (Mpro): Molecular docking, molecular dynamics, and QM/MM approaches. *Journal of Molecular Graphics and Modelling*, *126*, 108662. https://doi.org/10.1016/j.jmgm.2023.108662
58. Phutietsile, G. O., Fotaki, N., & Nishtala, P. S. (2024). Assessing the anticholinergic cognitive burden classification of putative anticholinergic drugs using drug properties. *British Journal of Clinical Pharmacology*, *90*(9), 2236–2255. https://doi.org/10.1111/bcp.16123